RM No. A7A29

NACA

RESEARCH MEMORANDUM

for the

Air Materiel Command, Army Air Forces

HIGH-SPEED WIND-TUNNEL TESTS OF A MODEL OF THE LOCKHEED YP-80A AIRPLANE INCLUDING CORRELATION WITH FLIGHT TESTS AND TESTS OF DIVE-RECOVERY FLAPS

By Joseph W. Cleary and Lyle J. Gray

Ames Aeronautical Laboratory
Moffett Field, Calif.

NATIONAL ADVISORY COMMITTEE FOR AERONAUTICS

WASHINGTON

FEB 14 1947

NACA RM No. A7A29

NATIONAL ADVISORY COMMITTEE FOR AERONAUTICS

RESEARCH MEMORANDUM

for the

Air Materiel Command, Army Air Forces

HIGH-SPEED WIND-TUNNEL TESTS OF A MODEL OF THE LOCKHEED YP-80A AIRPLANE INCLUDING CORRELATION WITH FLIGHT TESTS AND TESTS OF DIVE-RECOVERY FLAPS

By Joseph W. Cleary and Lyle J. Gray

SUMMARY

This report contains the results of tests of a 1/3-scale model of the Lockheed YP-80A "Shooting Star" airplane and a comparison of drag, maximum lift coefficient, and elevator angle required for level flight as measured in the wind tunnel and in flight. Included in the report are the general aerodynamic characteristics of the model and of two types of dive-recovery flaps, one at several positions along the chord on the lower surface of the wing and the other on the lower surface of the fuselage.

The results show good agreement between the flight and wind-tunnel measurements at all Mach numbers. The results indicate that the YP-80A is controllable in pitch by the elevators to a Mach number of at least 0.85. The fuselage dive-recovery flaps are effective for producing a climbing moment and increasing the drag at Mach numbers up to at least 0.8. The wing dive-recovery flaps are most effective for producing a climbing moment at 0.75 Mach number. At 0.85 Mach number, their effectiveness is approximately 50 percent of the maximum. The optimum position for the wing dive-recovery flaps to produce a climbing moment is at approximately 35 percent of the chord.

INTRODUCTION

At the request of the Air Materiel Command, U. S. Army Air Forces, high-speed wind-tunnel tests have been conducted of a 1/3-scale model of the Lockheed YP-80A "Shooting Star" airplane. The purpose of these tests was to furnish longitudinal-control data at high subsonic Mach numbers for correlation with flight-test results.

The YP-80A, as illustrated in figure 1, is a slightly modified version of the XP-80 airplane; the modifications include changes in the duct inlets, enlarging the center fuselage section, rounding the tips of the wing and the tail surfaces, extending the leading-edge fillets, dynamically mass-balancing the elevator, and increasing the elevator area. To these changes, together with an improved method of tunnel calibration and model support used in the present investigation, can be attributed the discrepancies that exist between the results of this test and those of previous model tests.

This investigation has been conducted over a Mach number range between 0.3 and 0.85 and a Reynolds number range between 4,180,000 and 7,610,000. The Reynolds number range, as illustrated by figure 2, is approximately equivalent to that of the airplane in flight at 40,000 feet altitude.

The tests were conducted in the Ames 16-foot high-speed wind tunnel, Moffett Field, Calif., and were witnessed by Mr. Frank Duschik of the Lockheed Aircraft Corporation.

SYMBOLS

The symbols used in this report are defined as follows:

V	free-stream velocity, feet per second
ρ	free-stream mass density, slugs per cubic foot
q	free-stream dynamic pressure $(\frac{1}{2}\rho V^2)$, pounds per square foot
M	Mach number
M_{cr}	critical Mach number (the free-stream Mach number at which the flow over the model first reaches the local speed of sound)
R	Reynolds number
S	wing area, square feet
M.A.C.	mean aerodynamic chord, feet
b_e	elevator span, feet
$\overline{c_e^2}$	elevator mean-square chord aft of hinge line, square feet
C_D	drag coefficient $\left(\frac{\text{drag}}{qS}\right)$
C_L	lift coefficient $\left(\frac{\text{lift}}{qS}\right)$

C_m pitching-moment coefficient $\left(\frac{\text{pitching moment}}{qS \quad \text{M.A.C.}}\right)$

C_{h_e} elevator hinge-moment coefficient $\left(\frac{\text{elevator hinge moment}}{q \; b_e \; c_e^2}\right)$

ΔC_D increase in drag coefficient

ΔC_m increase in pitching-moment coefficient

ΔC_{h_e} increase in elevator hinge-moment coefficient

α angle of attack of the fuselage reference line, degrees

α_o angle of attack of the fuselage reference line for zero lift, degrees

α_u uncorrected angle of attack of the fuselage reference line, degrees

$\Delta\alpha$ increase in angle of attack, degrees

δ_e elevator angle with respect to the stabilizer chord, degrees

δ_f dive-recovery flap angle with respect to the surface (wing or fuselage) at point of flap attachment, degrees

δ_t elevator tab angle with respect to the elevator chord, degrees

i_t stabilizer angle with respect to the fuselage reference line, degrees

Δi_t increase in stabilizer angle, degrees

g indicated acceleration of gravity, 32.2 feet per second per second

p_l local static pressure on the model, pounds per square foot

p_s free-stream static pressure, pounds per square foot

P pressure coefficient $\left(\frac{p_l - p_s}{q}\right)$

P_{cr} critical pressure coefficient (the pressure coefficient which corresponds to the local velocity of sound)

MODEL AND APPARATUS

A 1/3-scale model of the YP-80A airplane furnished by the Lockheed Aircraft Corporation was used to conduct this investigation. The fuselage was constructed of wood and sheet steel with a steel spar and framework. The wing had a maple leading edge and an aluminum trailing edge and contained a steel box spar covered with mahogany. The horizontal and vertical stabilizers and the control surfaces were machined from aluminum alloy.

The model was mounted on four 5-percent-thick front struts and a 7-percent-thick rear strut as illustrated by figure 3. The angle of attack of the model was varied remotely by vertical motion of the rear strut. In order to minimize variations in the tare drag, transition was fixed on the support struts at 15 percent of their chord.

The choking Mach number of the wind tunnel with the model mounted on the struts was estimated to be 0.87.

Forces and moments acting on the model were recorded by mechanical balances. Elevator hinge moments were computed from measurements of the strain of a steel cantilever with an electric strain gage. Elevator angles were remotely varied and the elevator positions were measured with an autosyn indicator.

Air was brought into the fuselage through inlets on each side of the fuselage forward of the wing-fuselage juncture and discharged at the tail of the model. The rate of air flow into the ducts was regulated to simulate high-speed level-flight conditions by varying the area of openings in grids within the fuselage. Measurements of total and static pressures at the duct entrance and exit were used to evaluate the rate of air flow.

Dive-recovery flaps were tested on the lower surface of the wing and fuselage as illustrated in figure 4. The wing dive-recovery flaps had a chord of 1.80 inches (model dimension) and extended along the span from 21.00 inches to 33.00 inches from the model center line.

Two fuselage flaps, each having a chord of 8.75 inches and a span of 5.44 inches (model dimensions), were located symmetrically with respect to the fuselage reference line. The flaps conformed with the fuselage contour when fully retracted. As the flaps were lowered 80°, the hinge line moved from 5.45 percent of the wing-root chord ahead of the leading edge to 6.26 percent aft of the leading edge.

The complete model consisted of a wing and fuselage with fillets and ducts, pilot enclosure, and a horizontal and vertical tail with a dorsal fin. Accessories were added, for drag

comparison purposes, to make the model identical with the airplane used in the flight tests. These accessories included an airspeed boom, a pitch, yaw, and temperature boom, a droppable fuel-tank mooring, a standard pitot, and a radio antenna.

The elevator had a constant-radius leading edge about the hinge line with flat surfaces extending from the hinge line to the trailing edge. The elevator hinge line was perpendicular to the fuselage reference line and at 75 percent of the chord of the horizontal tail. The gap between the elevator and stabilizer was unsealed.

The principal dimensions of the model were as follows:

Wing

Span	13.00 ft
Area	26.33 sq ft
M.A.C.	2.24 ft
Dihedral	$3^{\circ}40'$
Root section	NACA.65_1-213,a=0.5
Tip section	NACA 65_1-213,a=0.5
Root incidence	1°
Tip incidence	$-\frac{1}{2}^{\circ}$
Taper ratio $\left(\frac{\text{tip chord}}{\text{root chord}}\right)$	0.380

Horizontal Tail

Span	5.19 ft
Area (total)	4.84 sq ft
Dihedral	0°
Section	NACA 65-010
Incidence	$1\frac{1}{2}^{\circ}$
Taper ratio $\left(\frac{\text{tip chord}}{\text{root chord}}\right)$	0.308
Tail length (25 percent of the M.A.C. to the elevator hinge line)	5.49 ft

Elevator mean-square chord aft of hinge line . . . . 0.0577 sq ft

Elevator area aft of hinge line . . . . . 0.970 sq ft

Vertical Tail

Span . . . . . 2.14 ft

Area (total) . . . . . 2.49 sq ft

Section . . . . . NACA 65-010

Incidence . . . . . 0°

Taper ratio $\left(\frac{\text{tip chord}}{\text{root chord}}\right)$ 0.400

Rudder mean-square chord aft of hinge line . . . . 0.106 sq ft

Rudder area aft of hinge line . . . . . 0.583 sq ft

Ducts

Entrance area (both ducts) . . . . . 0.319 sq ft

Exit area . . . . . 0.217 sq ft

REDUCTION OF DATA

The following corrections have been applied to the data to compensate for tunnel-wall effects according to the method of reference 1:

$$\Delta\alpha = 1.040\ C_L, \text{ degrees}$$

$$\Delta C_D = 0.0181\ C_L^2$$

$$\Delta C_m = -0.497\ C_L \left(\frac{\partial C_m}{\partial i_t}\right)_M$$

A correction for flow inclination calculated from the shift in the angle of zero lift obtained from data with the model erect and inverted has been applied to the angle-of-attack and drag-coefficient data as follows:

$$\Delta\alpha = 0.2^\circ$$

$$\Delta C_D = 0.0035\ C_L$$

In order to calibrate the wind tunnel, the dynamic pressure and Mach number were evaluated by measurements in the test section with

the struts in place. The measurements were made by the method described in reference 2 through the use of long booms incorporating static-pressure orifices and extending well forward of a transverse airfoil which supported them. Local Mach numbers were computed from the static-pressure readings. The wind-tunnel calibration was taken as the average of the local Mach numbers corrected for constriction due to the model according to the method of reference 2.

Corrections for tare forces and moments of the struts have been applied to the force and moment data. These tares were evaluated by combining the separate effects from tests made with and without the upper and lower front struts and the rear strut. Because of strength limitations of the front struts when in compression, complete tare data were not obtained at high Mach numbers. Extrapolations of the tare data were made when necessary. Consequently, the precision of the high-speed data is not known with certainty for the entire lift range. Complete tare data were obtained in the region of zero lift at all Mach numbers.

Unless otherwise noted, all pitching-moment data have been computed about a point on the fuselage reference line above a point at 25 percent of the mean aerodynamic chord.

DISCUSSION OF RESULTS

Aerodynamic Characteristics

The lift, drag, and pitching-moment relationships for the model are illustrated in figures 5 to 12. The minimum drag coefficient as shown by figure 5, which excludes the internal duct drag, is 0.0115 at 0.30 Mach number. At low lift coefficients between Mach numbers of 0.30 and 0.76, the drag characteristics remain essentially unchanged. As the Mach number increases above 0.76 there is a rapid rise in drag coefficient as shown in figure 8. A comparison of the drag coefficient for the airplane as measured in flight and for the complete model with accessories as measured in the wind tunnel is presented in figure 9 for the flight-test lift coefficients. The agreement of the flight and the wind-tunnel data is excellent at all Mach numbers of the test. The close agreement between the low-speed data may be partly fortuitous considering that the flight-test drag was computed from the thrust (the predominate force at low speed) taken from an engine calibration chart. The drag data at high Mach numbers are on a better basis for comparison because the flight-test drag was computed principally from gravitational components, jet thrust being of secondary importance. The flight results are taken from data previously issued in preliminary form. Refinements in calibration of the flight-test instruments have been made since the data were first issued.

The effect of Mach number on lift coefficient, as presented in figure 10, shows an increase in lift coefficient for a given angle of attack with increasing Mach number until the Mach number of lift divergence is reached, followed by a rapid decrease in lift coefficient. Also shown is a curve of maximum lift coefficient for the model trimmed for zero pitching moment and for the airplane as measured in flight. (See reference 3.) Because of the large lift loads acting on the model at high Mach numbers at the maximum lift coefficient (approximately 14,000 lb), the model was mounted on two vertical 5-percent-thick struts having greater strength than the four struts used during the remainder of the test. The agreement between the flight and wind-tunnel data is good for Mach numbers above 0.50 where the effect of Reynolds number is small. At low speed where scale effects predominate, larger maximum lift coefficients are expected for the full-scale airplane than for the model.

The lift curves for the model increase in slope with increasing Mach number at a lower rate than the $\frac{1}{\sqrt{1 - M^2}}$ increase predicted by Glauert's theory, as shown in figure 11. The Mach number of lift divergence is approximately 0.77, at zero lift coefficient and it is followed by a sudden decrease in lift-curve slope. The angle of attack for zero lift for the model remains unchanged at -1.5° until the Mach number of lift divergence is reached, above which it rapidly increases to a positive value.

These changes in the lift characteristics at high Mach numbers produce changes in the static longitudinal-stability and -control characteristics. Figure 12 presents the pitching-moment characteristics for the model with and without the tail for several lift coefficients. When no change in elevator angle was assumed, a diving tendency would be reached at approximately 0.77 Mach number, and this tendency would become more severe as the Mach number is increased. Associated with this diving tendency is an increase in static longitudinal stability. At 0.85 Mach number and 0.1 lift coefficient the static longitudinal stability is approximately 50 percent greater than the low-speed value. A region of static instability occurring at lift coefficients greater than 0.60 between Mach numbers of 0.70 and 0.775 may cause control difficulties which would be disconcerting to a pilot when maneuvering at high speeds. With the tail removed, there is a gradual decrease in the static longitudinal instability until a Mach number of 0.825 is reached. At 0.85 Mach number a reversal in the static longitudinal instability occurs between lift coefficients of -0.2 and 0.1. In general, the aerodynamic characteristics of the model at high speeds present longitudinal-control problems similar to those discussed in reference 4.

Longitudinal Control

The effectiveness of the elevators $-\left(\frac{d\Delta C_m}{d\delta_e}\right)$ to produce changes in trim at low speed is 0.0133 as shown in figure 13 and this value decreases only slightly at the higher Mach numbers. The elevator effectiveness $-\left(\frac{d\Delta C_m}{d\delta_d}\right)$ is not appreciably affected by deflecting the wing or fuselage dive-recovery flaps. The stabilizer effectiveness $-\left(\frac{d\Delta C_m}{d\Delta i_t}\right)$ which is approximately 0.027 at 0.30 Mach number, as shown by figure 14, is still increasing at 0.85 Mach number. Figure 15 presents the elevator hinge-moment coefficients. No large changes in $dC_{h_e}/d\delta_e$ occur with increasing Mach number. The rate of change of hinge-moment coefficient with increasing lift coefficient or angle of attack is small in absolute magnitude and changes from a negative to a positive value at Mach numbers above 0.75. Figure 16 shows that Mach number has only a slight effect in decreasing the elevator tab effectiveness $-(d\Delta C_{h_e}/d\delta_t)$.

Calculated stick forces required during the pull-ups are shown in figure 17 for three altitudes. The stick-force calculations were made on the assumption that no tabs, springs, or boost are connected in the control linkage and that the control system is mass-balanced. The effect of the tail damping moment due to curvilinear flight is considered. Unless otherwise noted, a wing loading of 50 pounds per square foot is assumed for all calculations, and the center of gravity is assumed to be on the fuselage reference line above the 25-percent point of the mean aerodynamic chord. The airplane is assumed to be trimmed at 450 miles per hour at 20,000 feet altitude. Figure 18 indicates that the airplane will be stable with the stick free at sea level for Mach numbers below 0.71 and at 40,000 feet for Mach numbers below 0.68. The airplane appears to have stick-fixed stability at sea level for Mach numbers below 0.53 and at 40,000 feet for Mach numbers below 0.72. The rapid increase in stick force at 0.8 Mach number is primarily caused by the increase in static longitudinal stability and the decrease in the pitching moment as shown by the curves of figure 6. A comparison of the elevator angle required for level flight is made in figure 19 between flight-test measurements (preliminary flight-test data with subsequent refinements in analysis) and wind-tunnel calculations. The flight-test measurements and the wind-tunnel calculations are made for a wing loading of 45 pounds per square foot with the center of gravity at 28 percent of the mean aerodynamic chord at an altitude of approximately 20,000 feet. The variation with Mach number is similar for the two cases. A smaller up-elevator angle is indicated by the wind-tunnel data at all Mach numbers. A break in the flight-test curve at 0.74 Mach number also is indicated in

the wind-tunnel curve at approximately the same Mach number. This irregularity is caused by a small increase in static longitudinal stability at this Mach number, as shown by the pitching-moment curves of figure 6. The agreement between the flight and wind-tunnel data is reasonable inasmuch as the elevator angles required are sensitive to irregularities in the manufacture and alinement of either the model or airplane.

The effect of changes in center-of-gravity location on the stick forces required during pull-ups at 20,000 feet is shown in figure 20 and the effect of these changes on the stick-force gradient is shown in figure 21. Changing the center of gravity from 25 to 30 percent of the mean aerodynamic chord reduces the stick-force gradient from 9 to 4 pounds per g at 0.75 Mach number and 20,000 feet altitude. An increase in stick-force gradient occurs at 0.75 Mach number for all center-of-gravity positions presented. The center-of-gravity position at which the static longitudinal stability is predicted to be neutral $-\frac{\partial C_m}{\partial C_L} = 0$, the neutral point with the stick fixed, is also presented in figure 21. Increasing the Mach number changes the neutral point with the stick fixed from approximately 31 percent of the mean aerodynamic chord at Mach numbers below 0.65 to 36 percent of the mean aerodynamic chord at a Mach number of 0.85.

From the longitudinal control data presented, it appears that the YP-80A airplane should have no difficulty with longitudinal control when recovering from a high-speed dive up to at least 0.85 Mach number, the limit of the test.

Wing Pressure Distribution

Measurements of pressure distribution, as presented in figure 22, were obtained at a wing station 26.00 inches from the center line of the model along the wing span. The effect of changing the attitude of the model for several Mach numbers is shown in figure 22, while the effect of changing the Mach number for two lift coefficients is shown in figure 23. For a constant lift coefficient, there is only a slight shift in the location of the peak pressure on the upper surface with increasing Mach number, but the peak pressure moves aft on the lower surface. Separation of the flow becomes more severe on both surfaces as the Mach number increases above 0.8.

Figure 24 shows the variation of maximum pressure coefficient for both the upper and lower wing surfaces for three lift coefficients. At zero lift, the critical Mach number (M_{cr}) is approximately 0.70, which is approximately 0.06 less than the Mach number of drag divergence as indicated by force-test data.

Dive-Recovery Flaps

The wing dive-recovery flaps are effective for producing a climbing moment, as indicated by figure 25. Their effectiveness is maximum at a Mach number of approximately 0.75 and rapidly decreases at Mach numbers above 0.80. The data indicate that the effectiveness may become negligible at a Mach number slightly greater than 0.85. Figure 26 shows that with the tail removed the increment of pitching moment becomes negative at approximately 0.74 Mach number with a 45° flap deflection. With the airplane in flight at high Mach numbers, this negative pitching-moment increment is balanced by a large download on the tail. Figure 27 presents data showing the effect of flap location along the chord on the effectiveness of dive-recovery flaps for producing a climbing moment. It appears that for the YP-80A airplane the optimum location for producing a climbing moment is at approximately 35 percent of the chord. However, this position also produces large diving moments at high Mach numbers with the tail removed, as shown in figure 28.

The drag increment from deflecting the wing dive-recovery flaps is presented in figure 29. At the higher Mach numbers, this increment increases at a faster rate with increasing Mach number than at lower speeds because of the increased separation on the upper surface of the wing, as indicated by figure 30.

The effect of wing dive-recovery flaps on the wing pressure distribution is shown in figure 30. At low Mach numbers there is little change in the upper-surface pressure distribution, but the flaps alter the lower-surface pressure distribution to produce the climbing moment shown in figure 26. At a Mach number of approximately 0.75 a combination of rearward shock movement and increasing separation on the upper surface produces a diving moment which overbalances the climbing moment resulting from the lower-surface pressure distribution.

The fuselage dive-recovery flaps produce climbing moments if large flap deflections are used, as shown in figure 31. With flap deflections of 40° or less there is relatively little effect. Their effectiveness is maintained at a Mach number of 0.80 with no indication of decreasing effectiveness. Figure 32 shows that, with the tail removed, the flaps maintain their effectiveness for producing climbing moments to a Mach number of 0.80. The flaps are also a powerful device for increasing the drag, as shown by figure 33. An 80° flap deflection at zero lift produces 100 percent or more increase in drag coefficient at all Mach numbers.

Figure 34 shows lift coefficients for trim, stick free, when the wing or fuselage dive-recovery flaps are deflected, and the lift coefficient required for level flight at several altitudes. With a

30° deflection of the wing dive-recovery flaps and the trim tabs set at 0°, an indicated acceleration of 4g would be obtained at 0.80 Mach number and 10,000 feet altitude. For the same Mach number and altitude, an 80° deflection of the fuselage dive-recovery flaps would produce an indicated acceleration of 5g.

CONCLUSIONS

The test results indicate the following:

1. The drag and maximum lift coefficient of the YP-80A model as measured at high speed in the Ames 16-foot high-speed wind tunnel are in good agreement with flight-test data for the YP-80A airplane.

2. Although a diving tendency will be reached at approximately 0.77 Mach number, the YP-80A airplane is controllable in pitch by the elevators to a Mach number of at least 0.85.

3. The YP-80A airplane will have a stable variation of stick force with speed below a Mach number of 0.71 at sea level and below 0.68 Mach number at 40,000 feet altitude when trimmed at 450 miles per hour and 20,000 feet altitude. The variation of elevator angle for trim with speed indicates stability below a Mach number of 0.53 at sea level and below a Mach number of 0.72 at 40,000 feet.

4. The fuselage dive-recovery flaps are effective for recovery from dives to a Mach number of at least 0.8. The speed of a dive will be noticeably reduced by the large increment of drag from the flaps.

5. The wing dive-recovery flaps are most effective for dive recovery at a Mach number of 0.75, but the effectiveness decreases at higher Mach numbers. The optimum location of these flaps for producing climbing moments when mounted on the YP-80A is at 35 percent of the chord.

6. It appears from an extrapolation of the data that, for the YP-80A airplane, the wing dive-recovery flaps may lose their effectiveness at a Mach number at which the elevators are still effective for controlling the airplane.

Ames Aeronautical Laboratory,
National Advisory Committee for Aeronautics,
Moffett Field, Calif.

Joseph W. Cleary,
Mechanical Engineer.

Lyle J. Gray,
Aeronautical Engineer.

Approved:

Donald H. Wood,
Aeronautical Engineer.

REFERENCES

1. Silverstein, Abe, and White, James A.: Wind-Tunnel Interference with Particular Reference to Off-Center Positions of the Wing and to the Downwash at the Tail. NACA Rep. No. 547, 1935.

2. Nisson, James M., Gadeberg, Burnett L., and Hamilton, William T.: Correlation of the Drag Characteristics of a P-51B Airplane Obtained from High-Speed Wind-Tunnel and Flight Tests. NACA ACR No. 4K02, 1945.

3. Spreiter, John R. and Steffen, Paul J.: Effect of Mach and Reynolds Numbers on Maximum Lift Coefficient. NACA TN No. 1044, 1946.

4. Hood, Manley J. and Allen, H. Julian: The Problem of Longitudinal Stability and Control at High Speeds. NACA CB No. 3K18, 1943.

FIGURE LEGENDS

Figure 1.— A three-view drawing of the YP-80A airplane.

Figure 2.— The Reynolds number for the YP-80A airplane in flight and for the 1/3-scale model in the Ames 16-foot high-speed wind tunnel.

Figure 3.— The 1/3-scale model of the YP-80A airplane mounted on the four-strut support system. (a) Front view. (b) Rear view.

Figure 4.— The wing and fuselage dive-recover flaps mounted on the 1/3-scale model of the YP-80A airplane. (a) Wing flaps. (b) Fuselage flaps.

Figure 5.— Variation of lift coefficient with drag coefficient for the complete 1/3-scale model of the YP-80A airplane.

Figure 6.— Variation of lift coefficient with angle of attack and pitching-moment coefficient with lift coefficient for the complete 1/3-scale model of the YP-80A airplane.

Figure 7.— Variation of lift coefficient with angle of attack and pitching-moment coefficient with lift coefficient for the 1/3-scale model of the YP-80A airplane less the tail.

Figure 8.— The variation of drag coefficient with Mach number for the complete 1/3-scale model of the YP-80A airplane.

Figure 9.— A comparison of the drag coefficient for the YP-80A airplane and the complete 1/3-scale model of the YP-80A with accessories at the flight test lift coefficient.

Figure 10.— Variation of lift coefficient with Mach number for the complete 1/3-scale model of the YP-80A airplane and a comparison of flight and wind-tunnel maximum lift coefficient data.

Figure 11.— Variation of the lift-curve slope and the angle of zero lift with Mach number for the complete 1/3-scale model of the YP-80A airplane.

Figure 12.— Variation of pitching-moment coefficient with Mach number for the 1/3-scale model of the YP-80A airplane.

Figure 13.— Elevator effectiveness for the complete 1/3-scale model of the YP-80A airplane. Tab angle, 0°.

Figure 14.– Stabilizer effectiveness for the complete 1/3-scale model of the YP-80A airplane. Elevator angle, 0°.

Figure 15.– Variation of elevator hinge-moment coefficient with elevator angle for the complete 1/3-scale model of the YP-80A airplane. Tab angle, 0°.

Figure 16.– Elevator tab effectiveness for the complete 1/3-scale model of the YP-80A airplane. (a) Elevator angle, 0°.

Figure 16.– Concluded. (b) Elevator angle, –6°.

Figure 17.– Calculated stick forces during pull-ups for the YP-80A airplane at three altitudes. Airplane trimmed at 450 miles per hour at 20,000 feet altitude.

Figure 18.– Calculated stick force and elevator angle required for level flight for the YP-80A airplane trimmed at 450 miles per hour at 20,000 feet altitude.

Figure 19.– A comparison of the elevator angle required for level flight for the YP-80A airplane and the complete 1/3-scale model of the YP-80A.

Figure 20.– Calculated stick forces during pull-ups for the YP-80A airplane for three center-of-gravity positions. Airplane trimmed at 450 miles per hour at 20,000 feet altitude.

Figure 21.– Variation of neutral point and stick force gradient for the YP-80A airplane.

Figure 22.– Pressure distribution over the wing of the complete 1/3-scale model of the YP-80A airplane. Wing station, 26.00 inches. (a) Mach number, 0.3

Figure 22.– Continued. (b) Mach number, 0.5.

Figure 22.– Continued. (c) Mach number, 0.6.

Figure 22.– Continued. (d) Mach number, 0.7.

Figure 22.– Continued. (e) Mach number, 0.75

Figure 22.– Continued. (f) Mach number, 0.8.

Figure 22.– Continued. (g) Mach number, 0.825.

Figure 22.– Concluded. (h) Mach number, 0.85.

Figure 23.– The effect of Mach number on the pressure distribution over the wing of the complete 1/3-scale model of the YP-80A airplane. (a) Lift coefficient, 0.

Figure 23.– Concluded. (b) Lift coefficient, 0.2.

Figure 24.– The variation of maximum pressure coefficient with Mach number for the complete 1/3-scale model of the YP-80A airplane. Wing station, 26.00 inches.

Figure 25.– The increment of pitching-moment coefficient from the wing dive-recovery flaps for the complete 1/3-scale model of the YP-80A airplane. Flap position, 35 percent of the M.A.C.

Figure 26.– The increment of pitching-moment coefficient from the wing dive-recovery flaps for the 1/3-scale model of the YP-80A airplane less the tail. Flap position, 35 percent of the M.A.C.

Figure 27.– The effect of flap location on the increment of pitching-moment coefficient from the wing dive-recovery flaps for the complete 1/3-scale model of the YP-80A airplane. Flap angle, 45°.

Figure 28.– The effect of flap location on the increment of pitching-moment coefficient from the wing dive-recovery flaps for the complete 1/3-scale model of the YP-80A airplane less the tail. Flap angle, 45°.

Figure 29.– The increment of drag coefficient from the wing dive-recovery flaps for the complete 1/3-scale model of the YP-80A airplane.

Figure 30.– The effect of wing dive-recovery flaps on the pressure distribution over the wing of the complete 1/3-scale model of the YP-80A airplane. Wing station, 26.00 inches; $\alpha_u, \frac{1}{2}°$.

Figure 31.– The increment of pitching-moment coefficient from the fuselage dive-recovery flaps for the complete 1/3-scale model of the YP-80A airplane.

Figure 32.– The increment of pitching-moment coefficient from the fuselage dive-recovery flaps for the 1/3-scale model of the YP-80A airplane less the tail.

Figure 33.— The increment of drag coefficient from the fuselage dive-recovery flaps for the complete 1/3-scale model of the YP-80A airplane.

Figure 34.— Calculated lift coefficient for trim, stick free, with the dive-recovery flaps and the lift coefficient required for level flight for the YP-80A airplane.

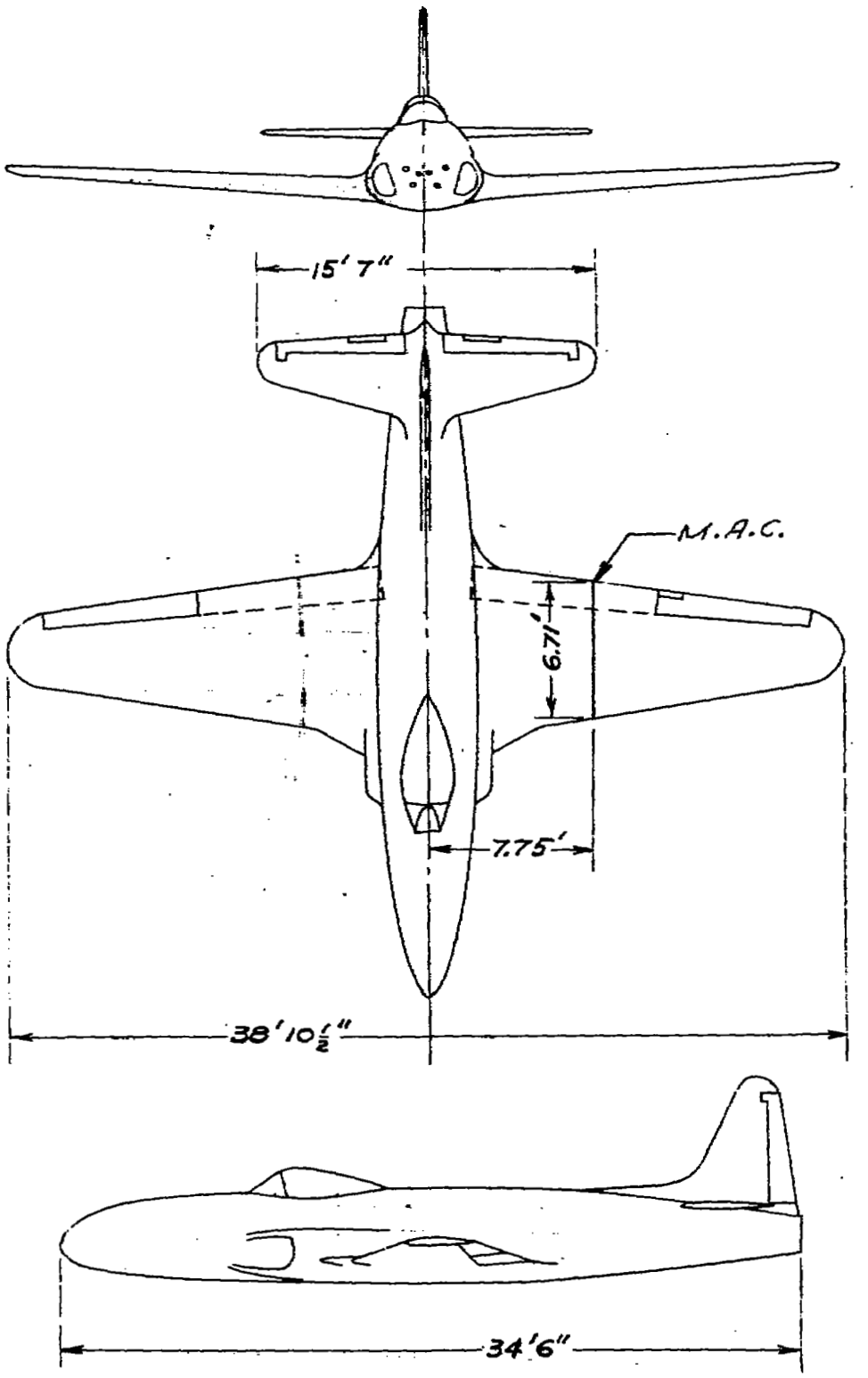

FIGURE 1.- A THREE-VIEW DRAWING OF THE YP-80A AIRPLANE

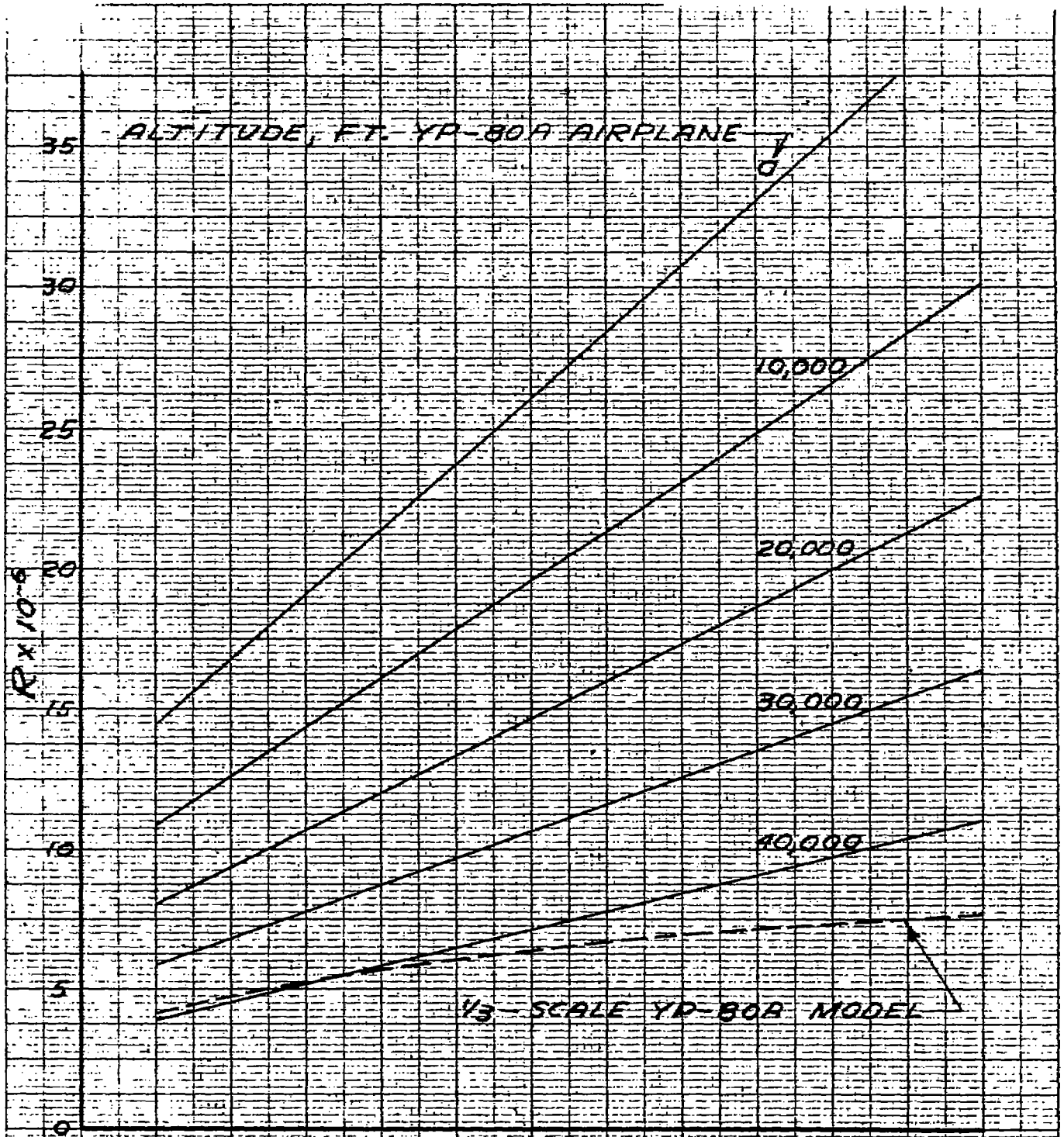

FIGURE 2.- THE REYNOLDS NUMBER FOR THE YP-80A AIRPLANE IN FLIGHT AND FOR THE 1/3-SCALE MODEL IN THE AMES 16-FOOT HIGH-SPEED WIND TUNNEL.

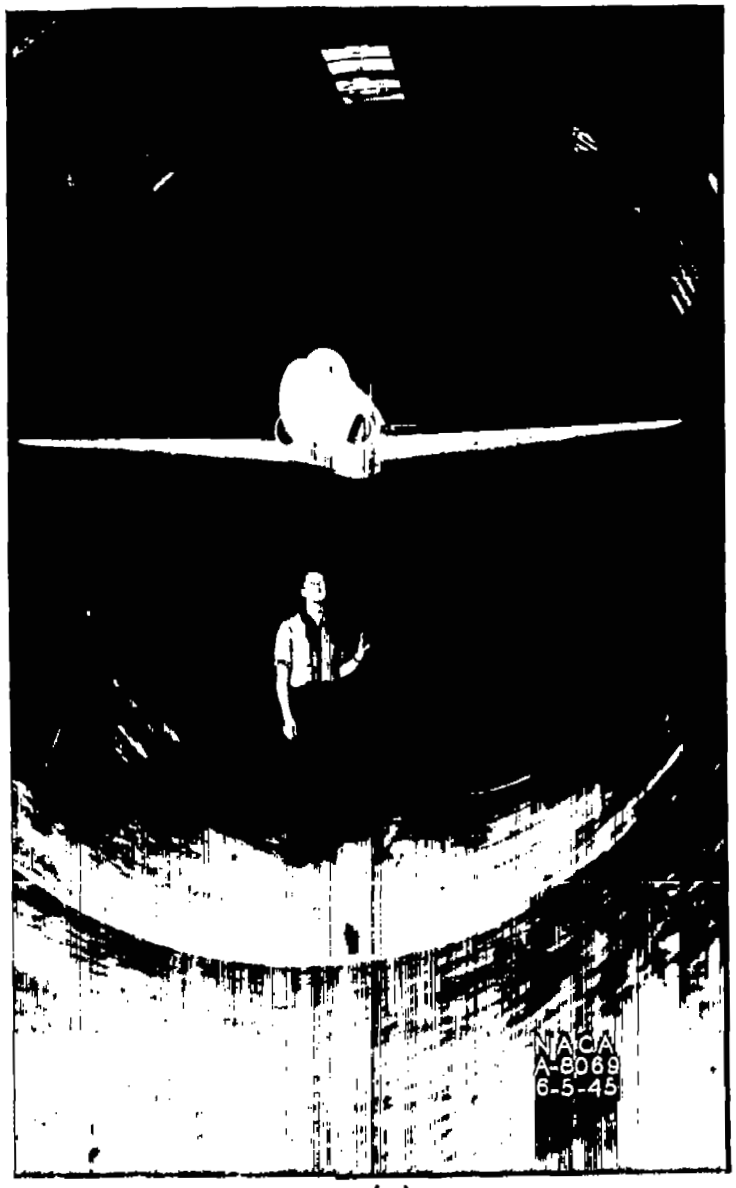

(a) Front View

(b) Rear View

Figure 3.- The 1/3-scale model of the YP-80A airplane mounted on the four-strut support system.

NATIONAL ADVISORY COMMITTEE FOR AERONAUTICS
AMES AERONAUTICAL LABORATORY — MOFFETT FIELD, CALIF.

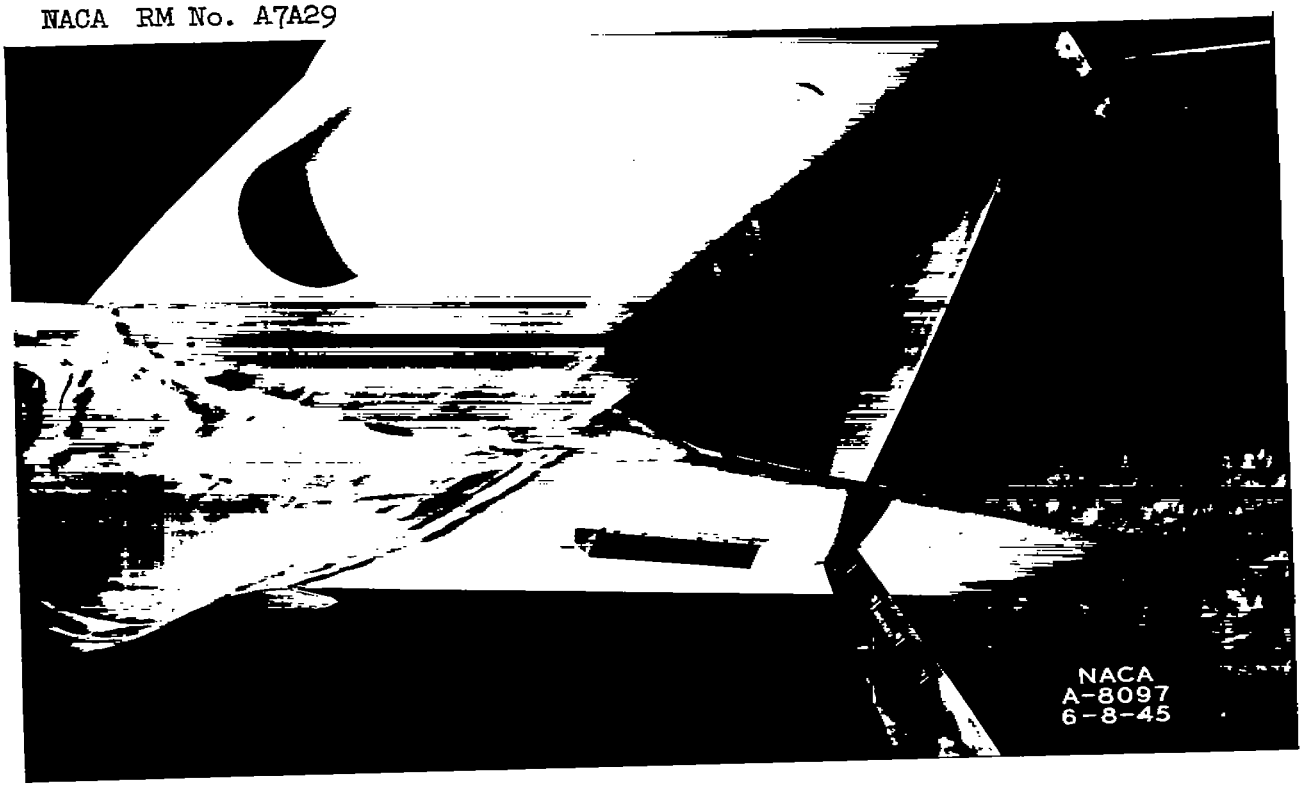

(a) Wing Flaps.

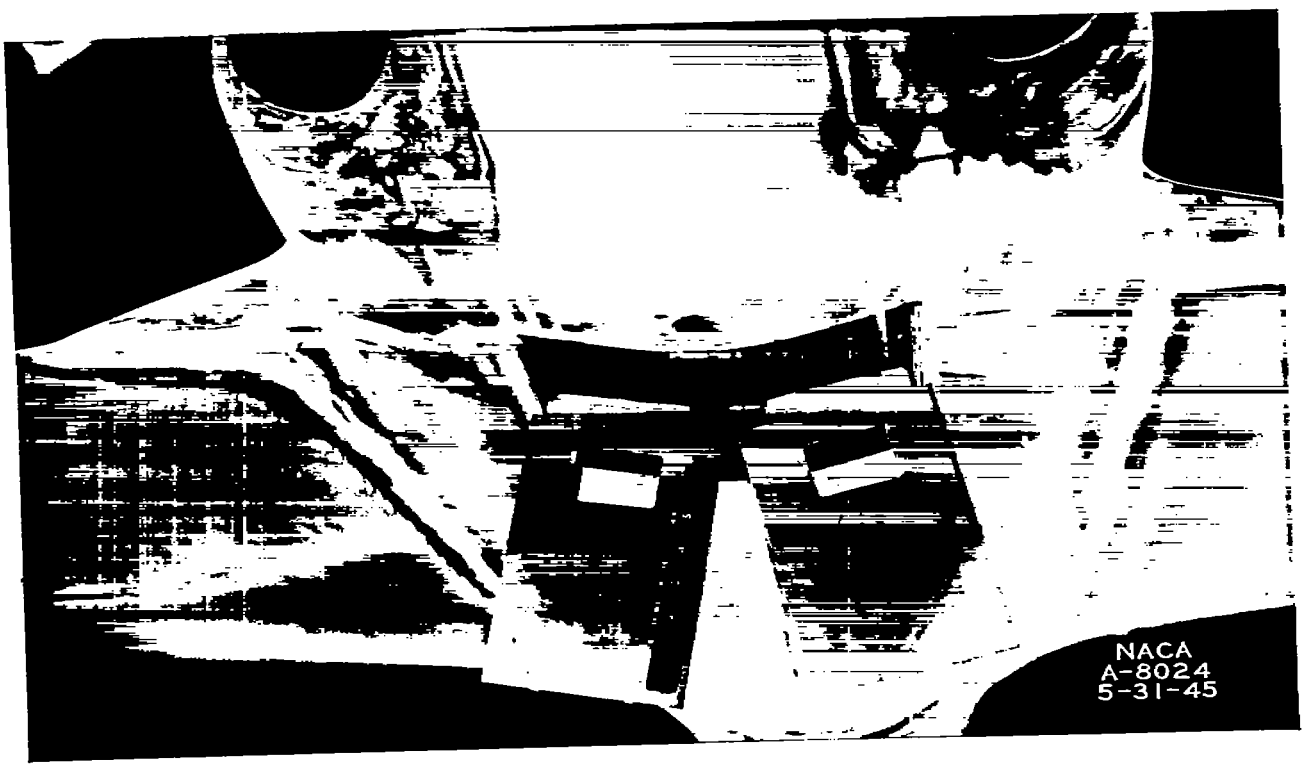

(b) Fuselage Flaps.

Figure 4.— The wing and fuselage dive-recovery flaps mounted on the 1/3- scale model of the YP-80A airplane.

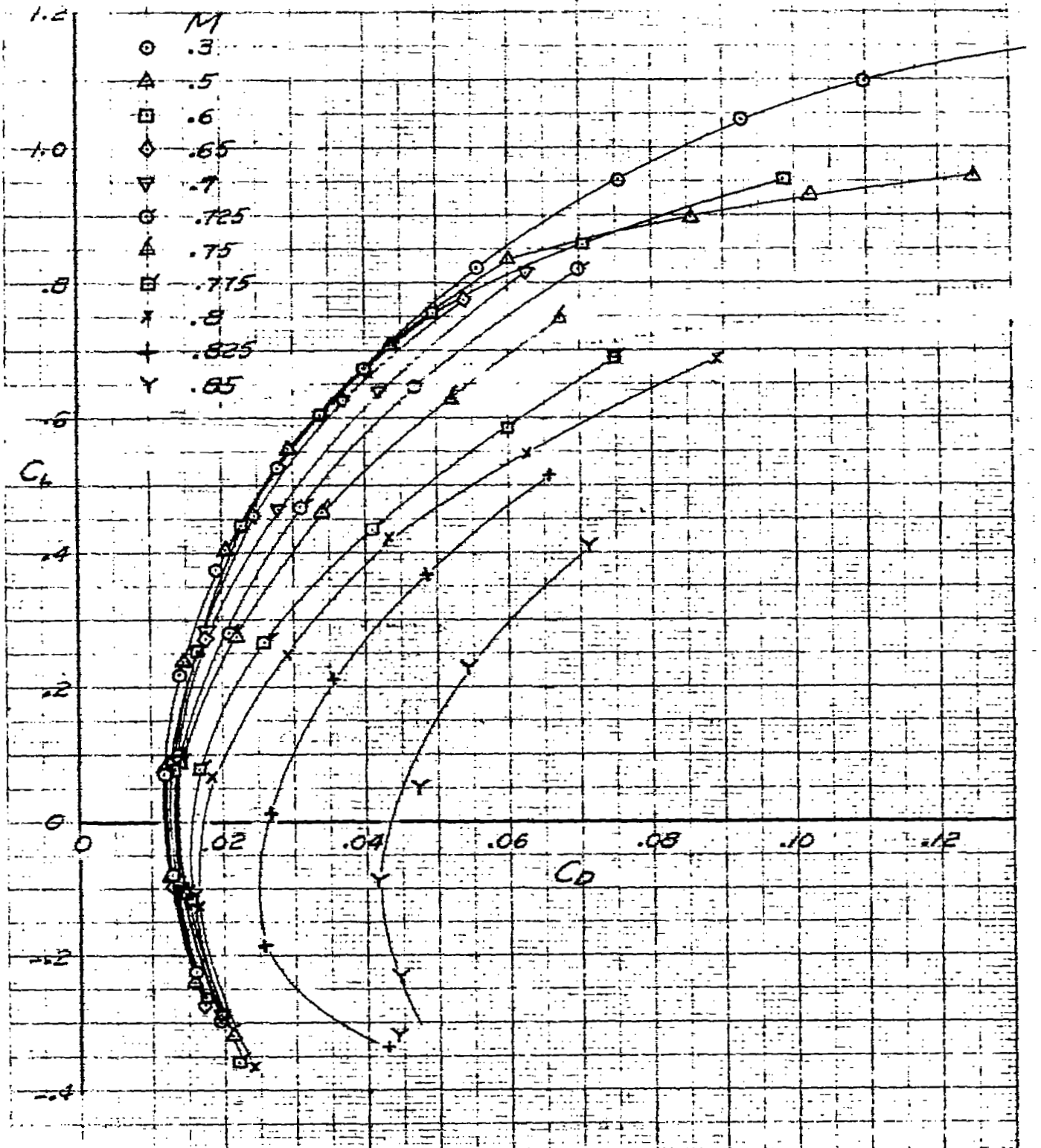

FIGURE 5.- VARIATION OF LIFT COEFFICIENT WITH DRAG COEFFICIENT FOR THE COMPLETE 1/3-SCALE MODEL OF THE YP-80A AIRPLANE.

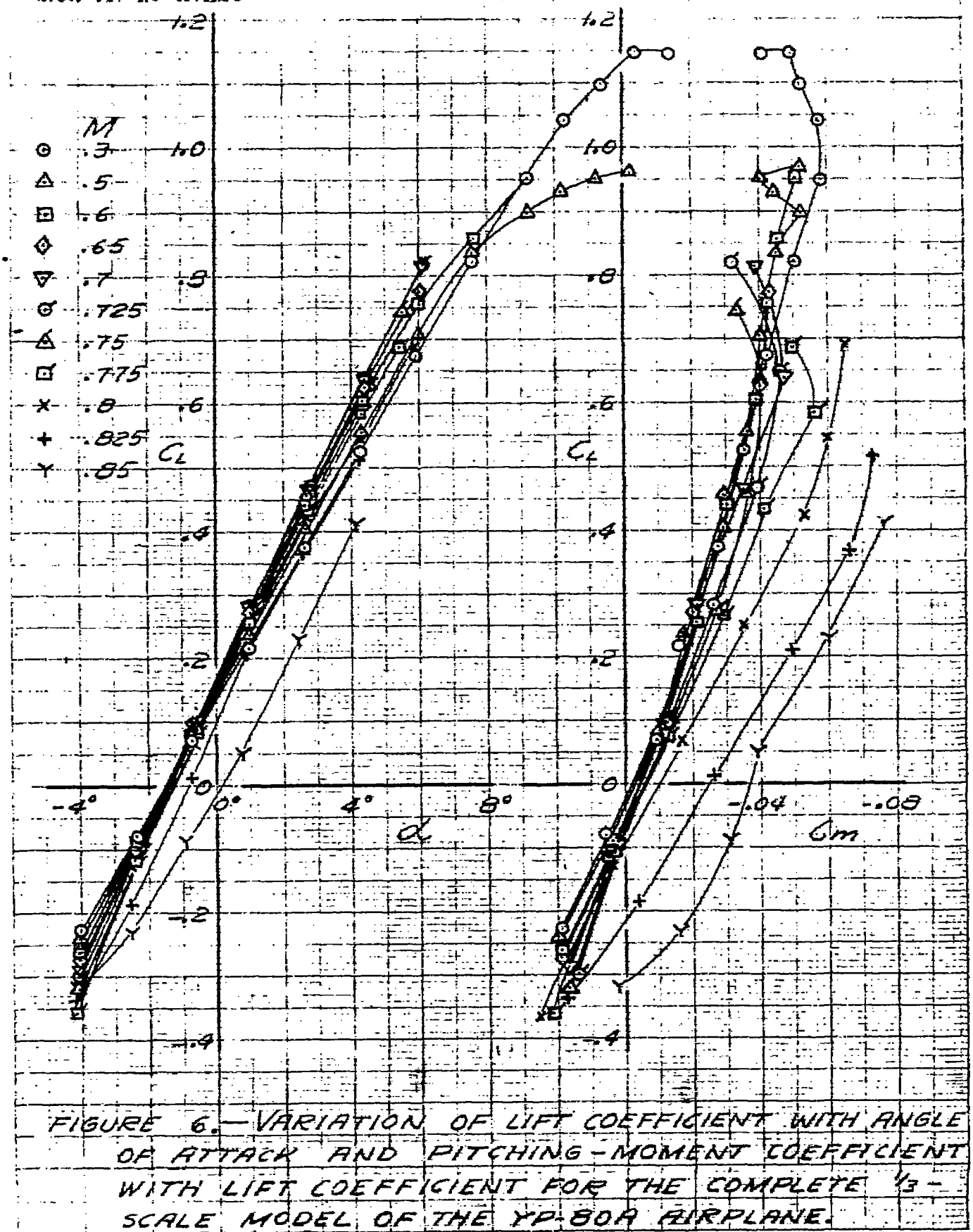

FIGURE 6.—VARIATION OF LIFT COEFFICIENT WITH ANGLE OF ATTACK AND PITCHING-MOMENT COEFFICIENT WITH LIFT COEFFICIENT FOR THE COMPLETE 1/3-SCALE MODEL OF THE YP-80A AIRPLANE.

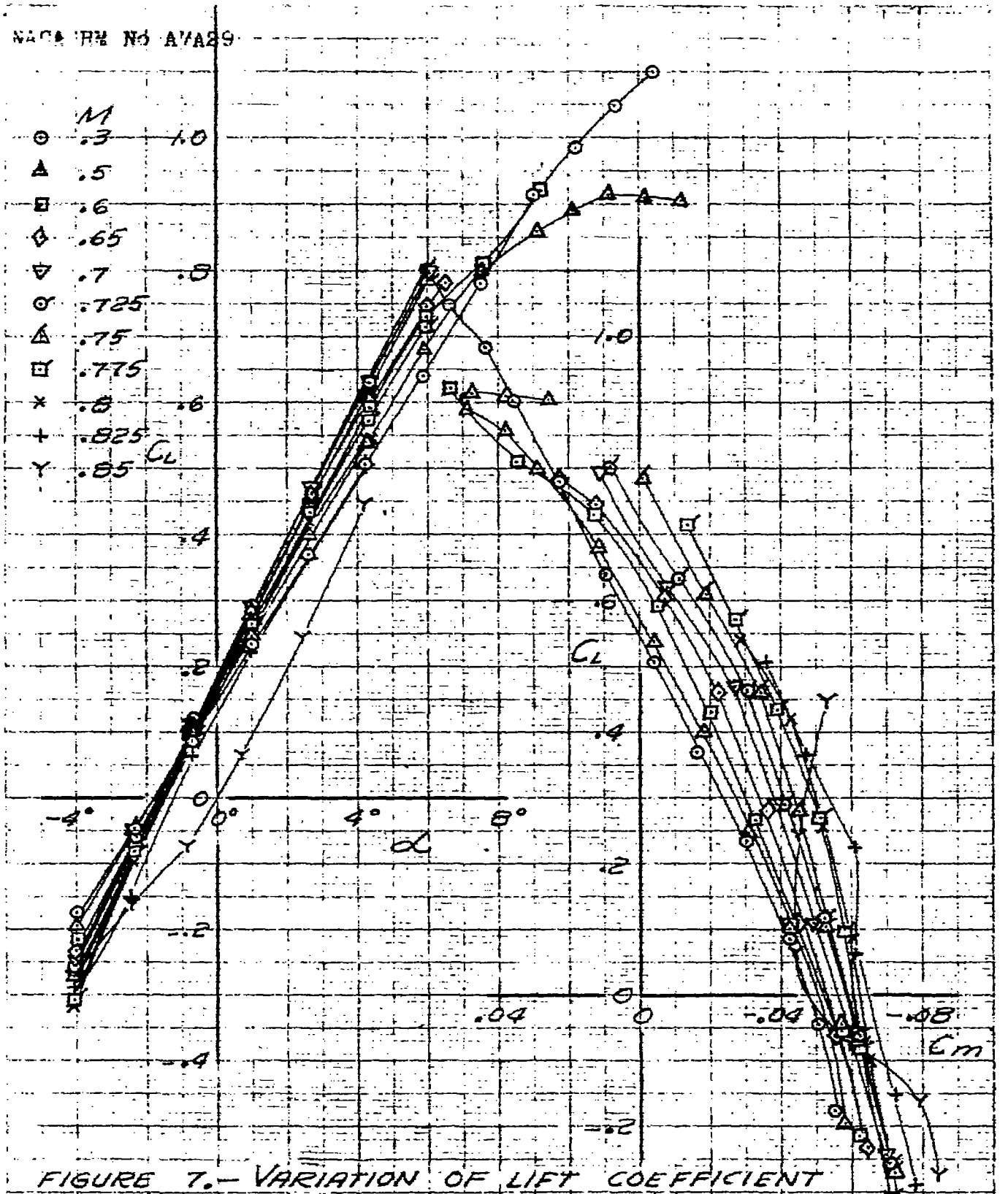

FIGURE 7.- VARIATION OF LIFT COEFFICIENT WITH ANGLE-OF-ATTACK AND PITCHING-MOMENT COEFFICIENT WITH LIFT COEFFICIENT FOR THE 1/3-SCALE MODEL OF THE YP-80A AIRPLANE LESS THE TAIL.

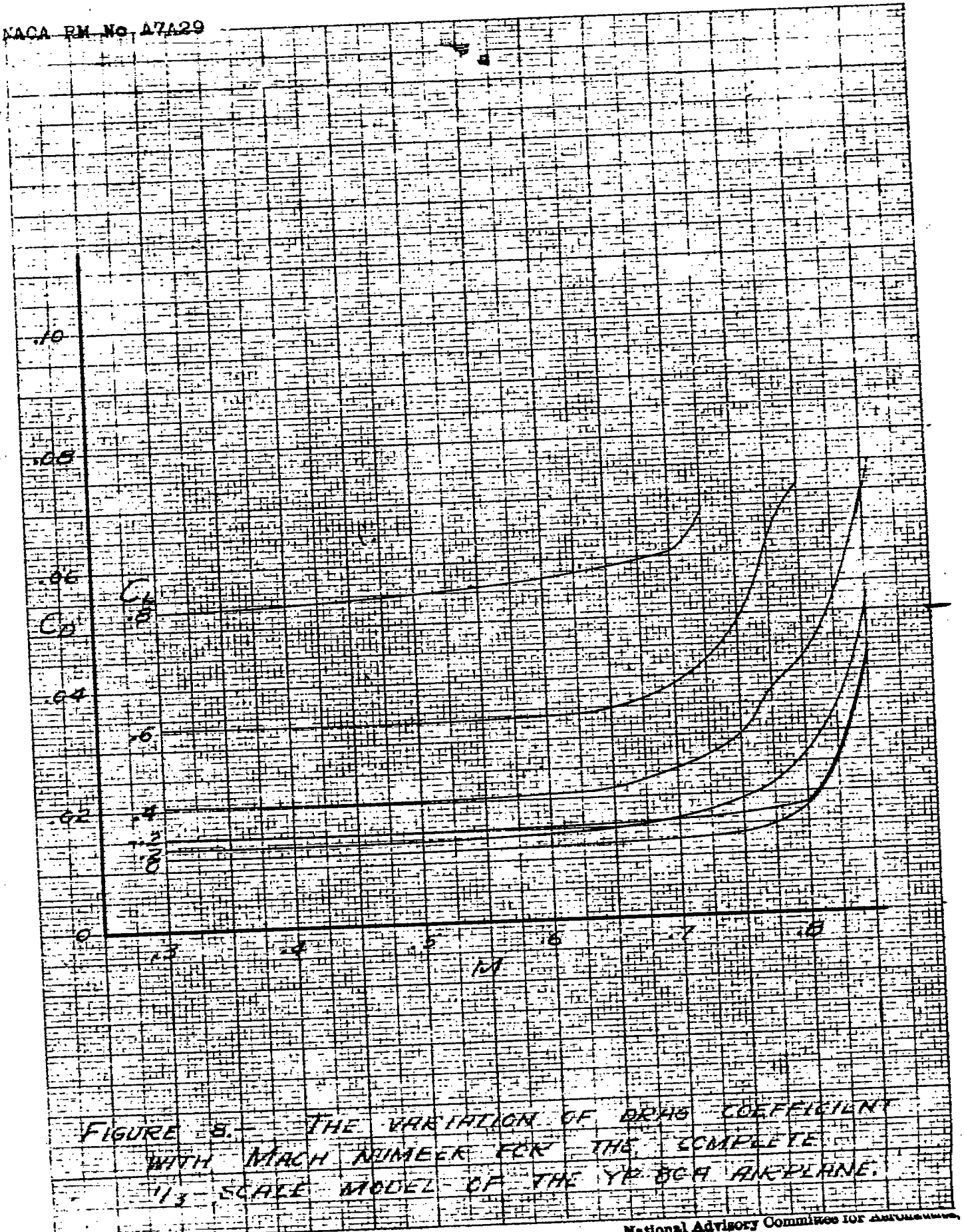

FIGURE 8.- THE VARIATION OF DRAG COEFFICIENT WITH MACH NUMBER FOR THE COMPLETE 1/3-SCALE MODEL OF THE YP-80A AIRPLANE.

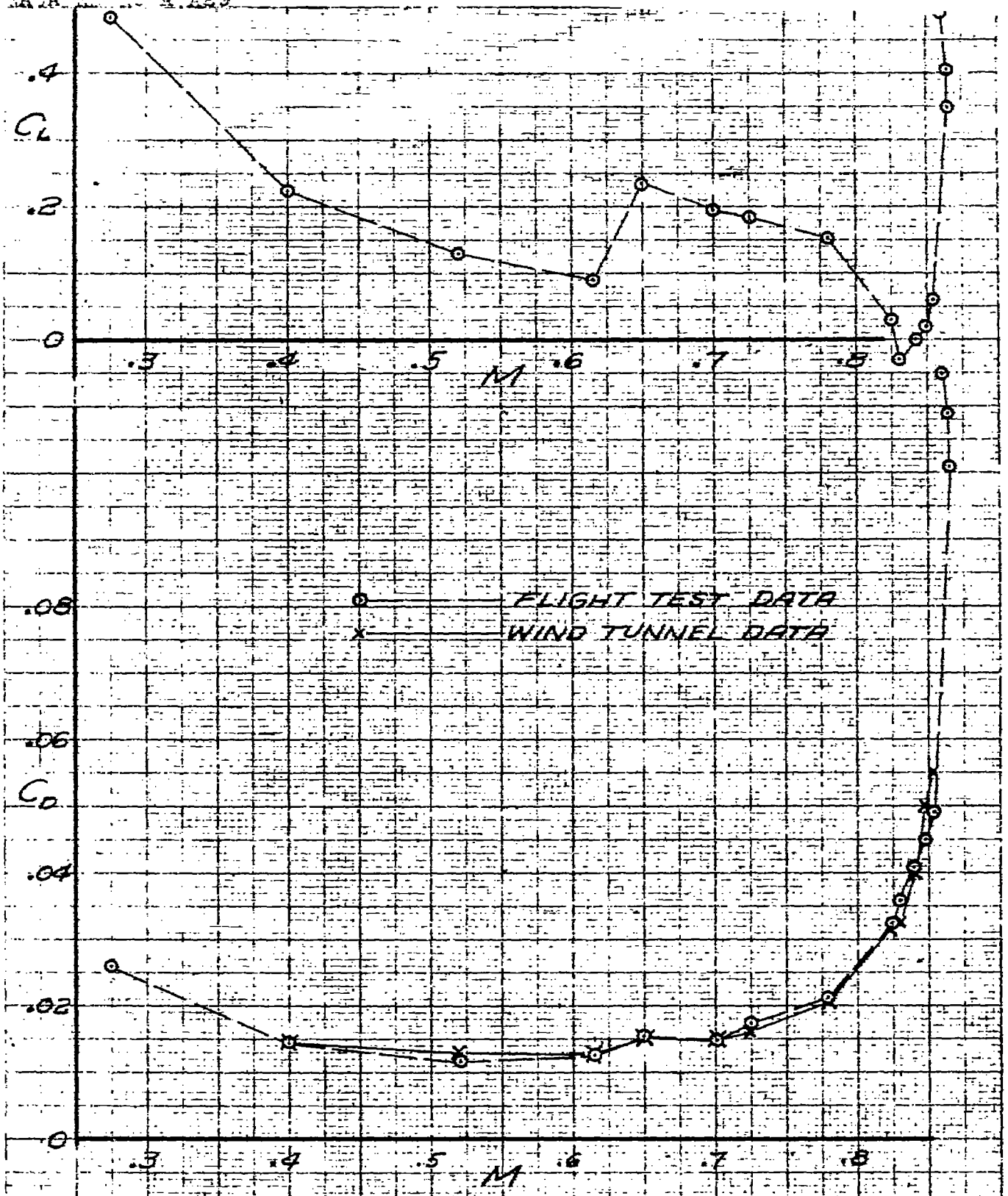

FIGURE 9.- A COMPARISON OF THE DRAG COEFFICIENT FOR THE YP-80A AIRPLANE AND THE COMPLETE 1/3-SCALE MODEL OF THE YP-80A WITH ACCESSORIES AT THE FLIGHT TEST LIFT COEFFICIENT.

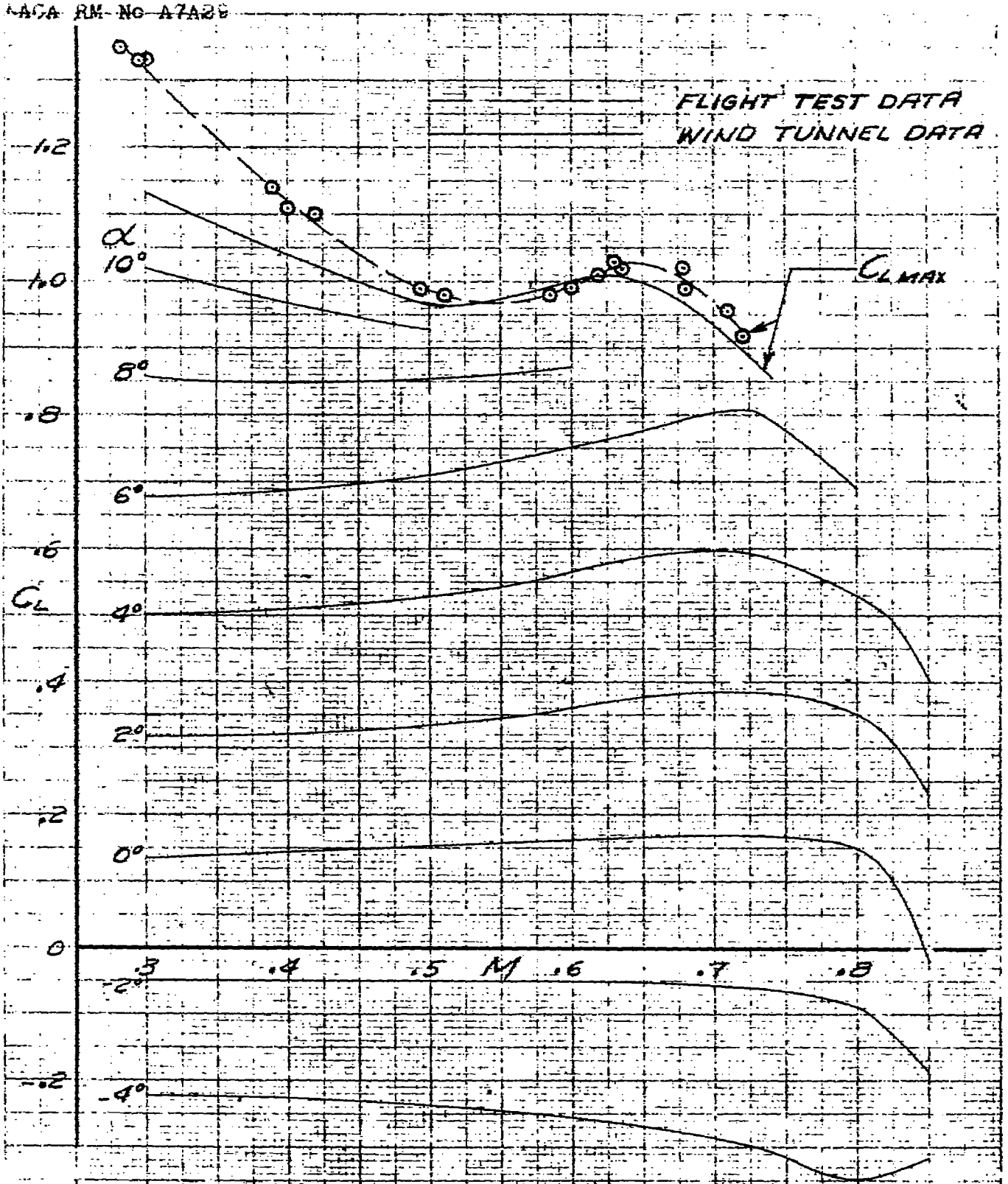

FIGURE 10.—VARIATION OF LIFT COEFFICIENT WITH MACH NUMBER FOR THE COMPLETE 1/3-SCALE MODEL OF THE YP-80A AIRPLANE AND A COMPARISON OF FLIGHT AND WIND TUNNEL MAXIMUM LIFT COEFFICIENT DATA.

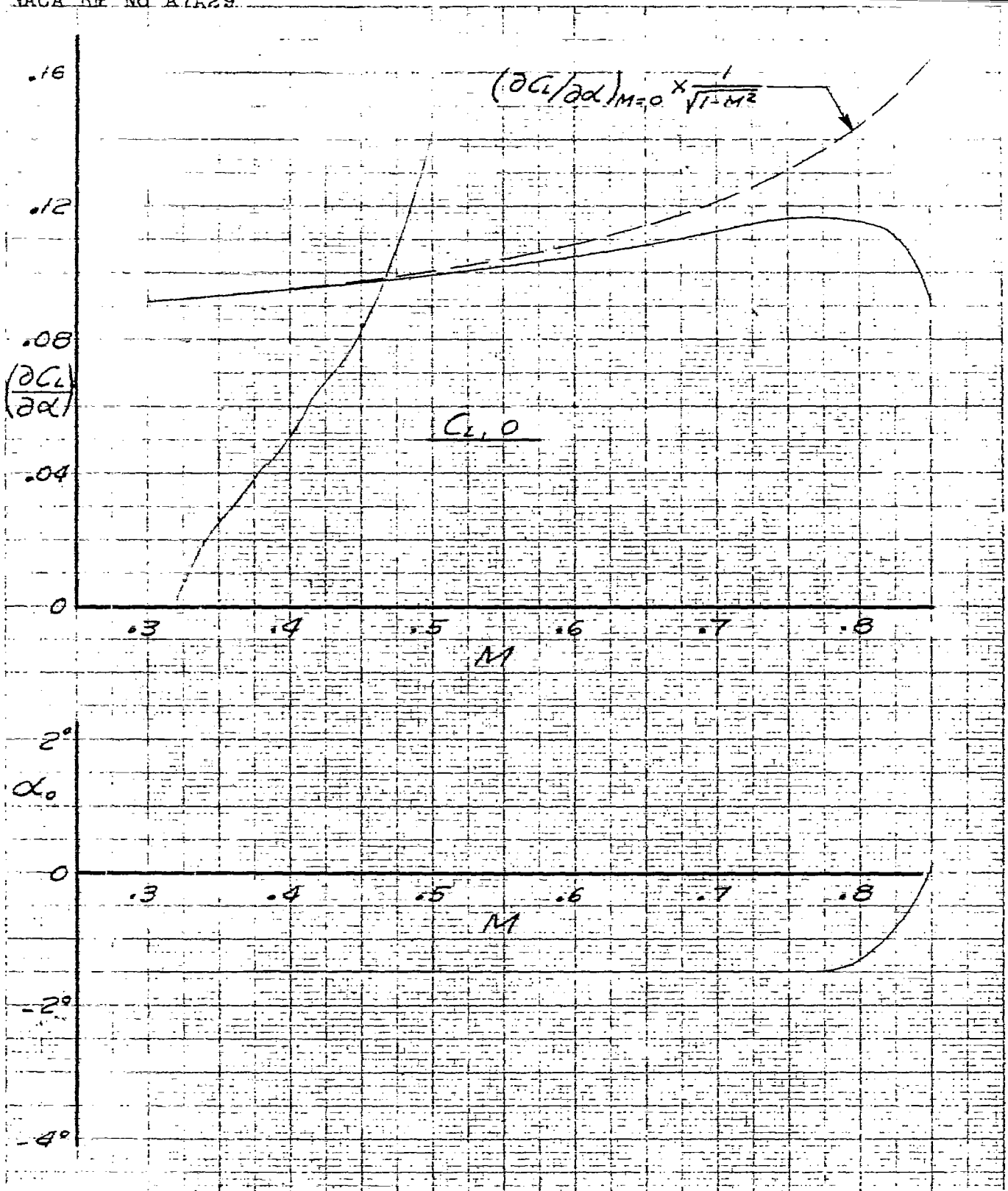

FIGURE 11.—VARIATION OF THE LIFT-CURVE SLOPE AND THE ANGLE OF ZERO LIFT WITH MACH NUMBER FOR THE COMPLETE 1/3-SCALE MODEL OF THE YP-80A AIRPLANE.

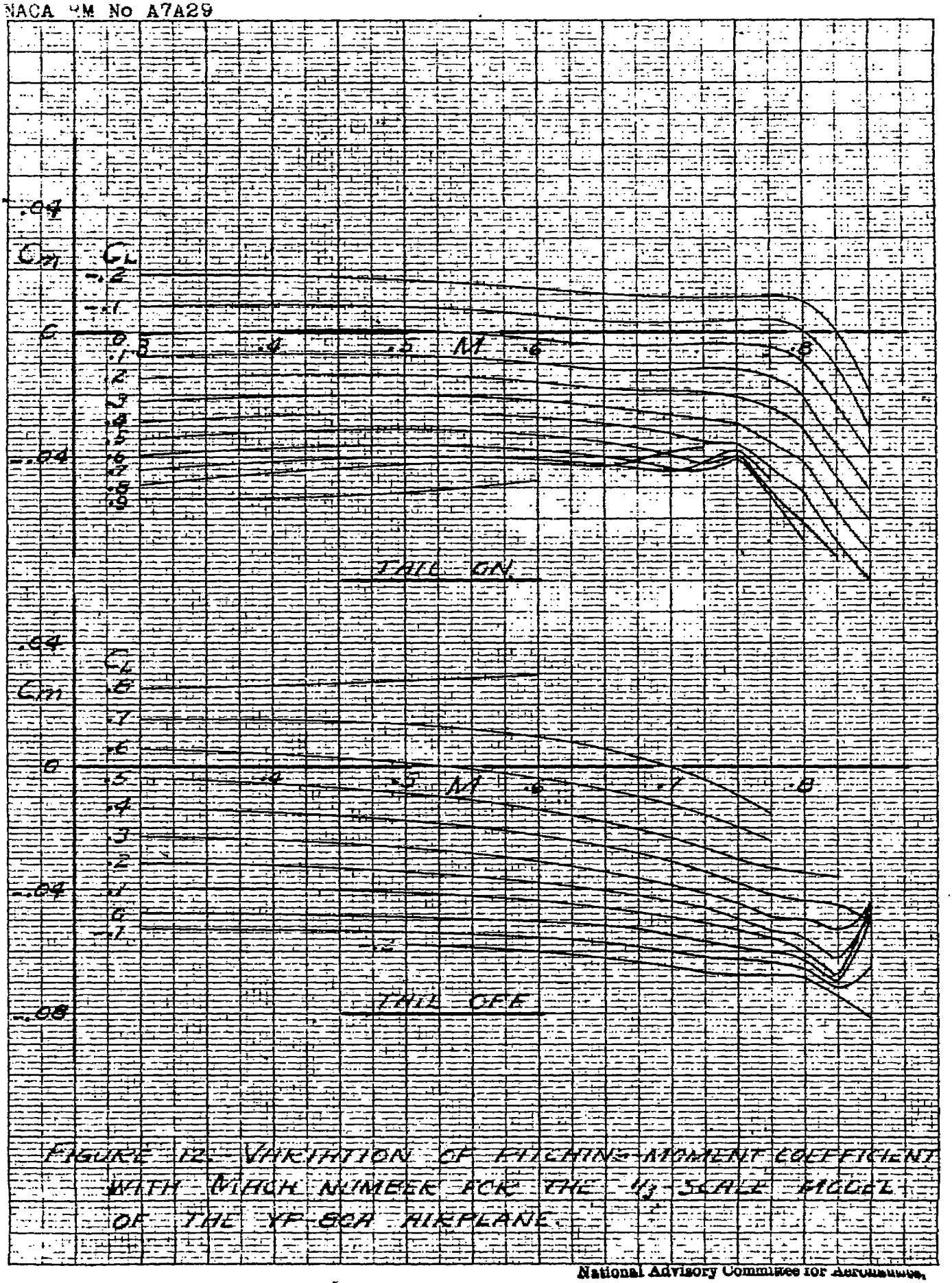

FIGURE 12.- VARIATION OF PITCHING-MOMENT COEFFICIENT WITH MACH NUMBER FOR THE 1/3-SCALE MODEL OF THE XF-88A AIRPLANE.

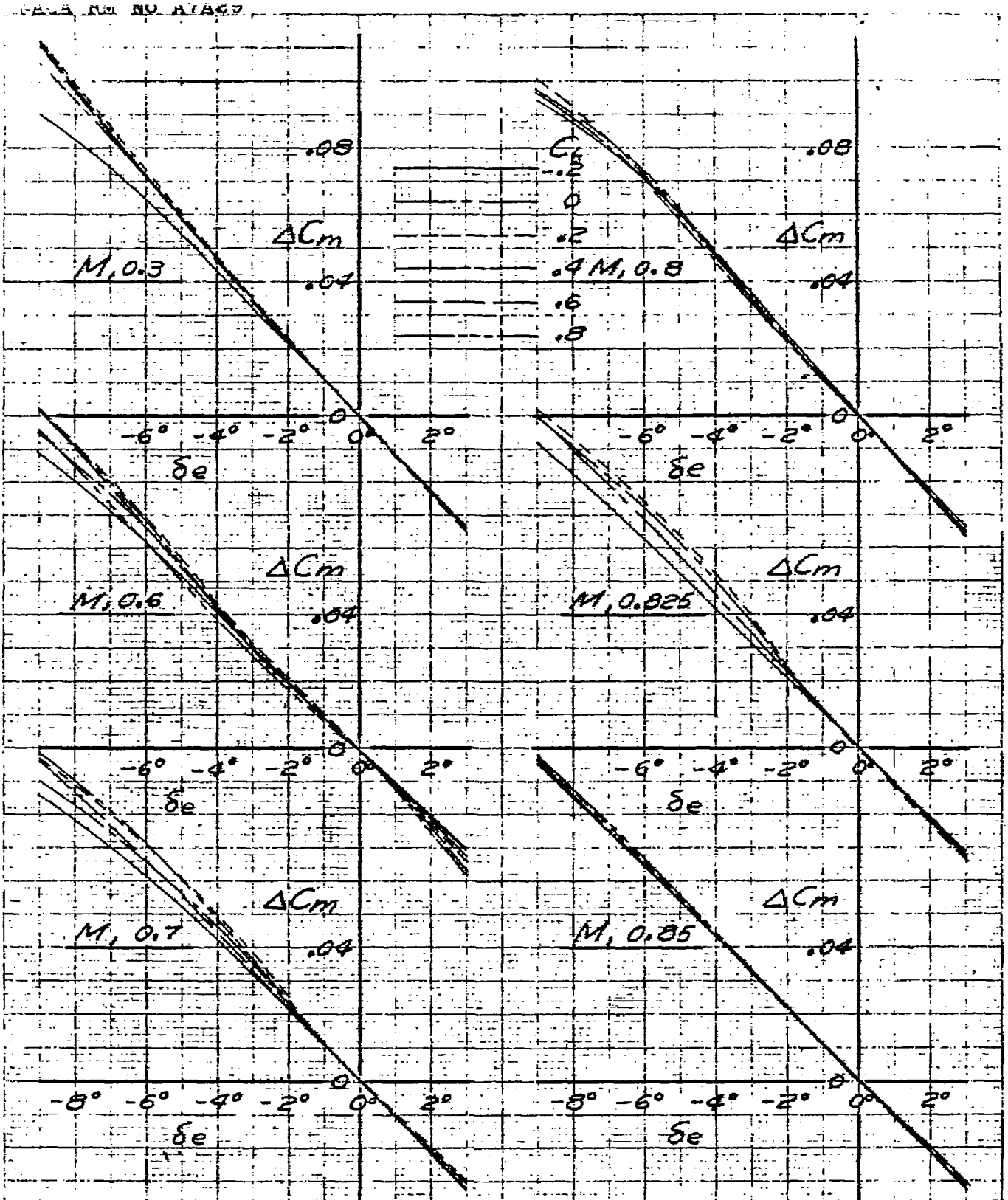

FIGURE 13.- ELEVATOR EFFECTIVENESS FOR THE COMPLETE 1/3-SCALE MODEL OF THE YP-80A AIRPLANE. TAB ANGLE, 0°

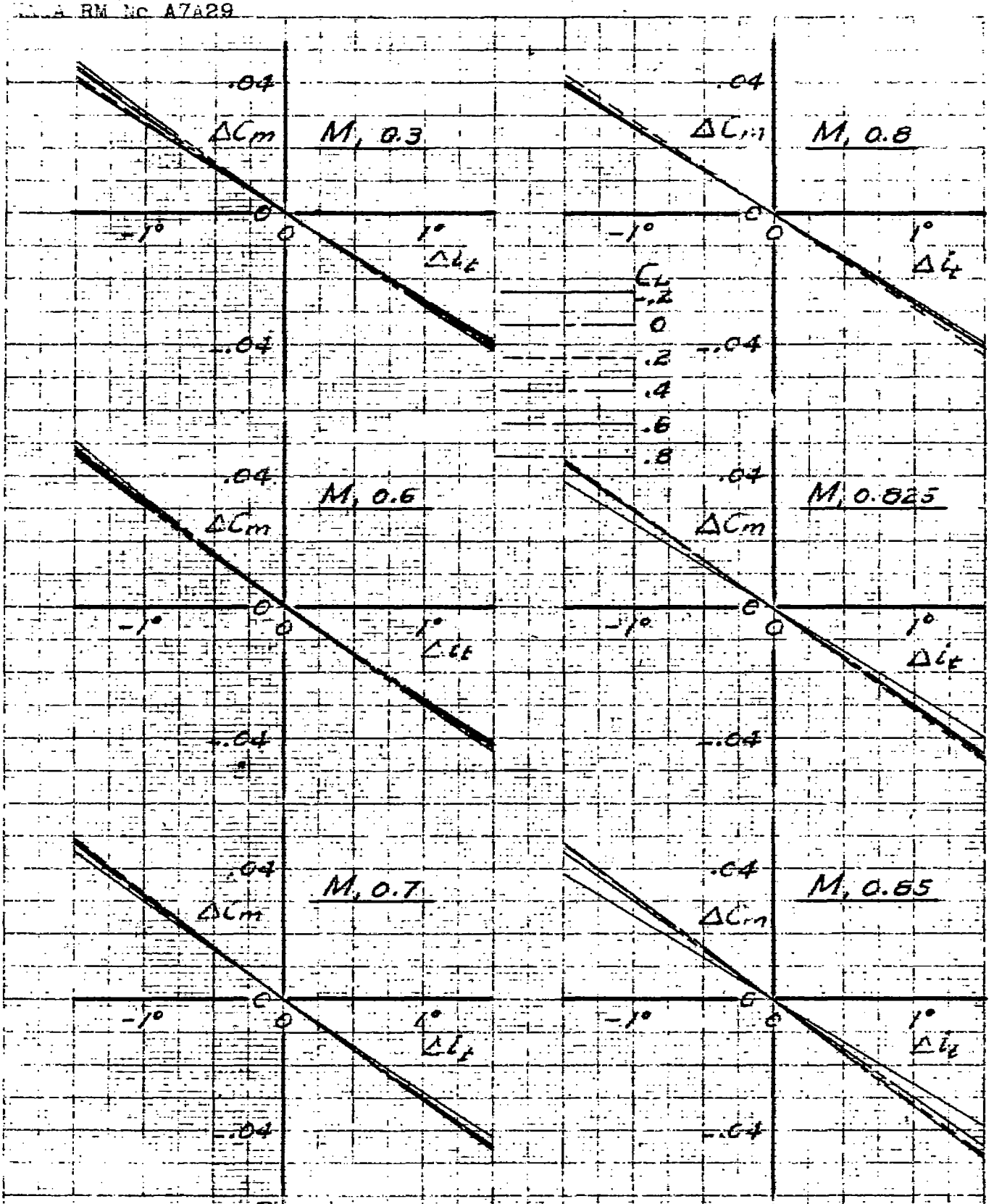

FIGURE 14.- STABILIZER EFFECTIVENESS FOR THE COMPLETE 1/3-SCALE MODEL OF THE YP 80A AIRPLANE. ELEVATOR HINGE, 0°

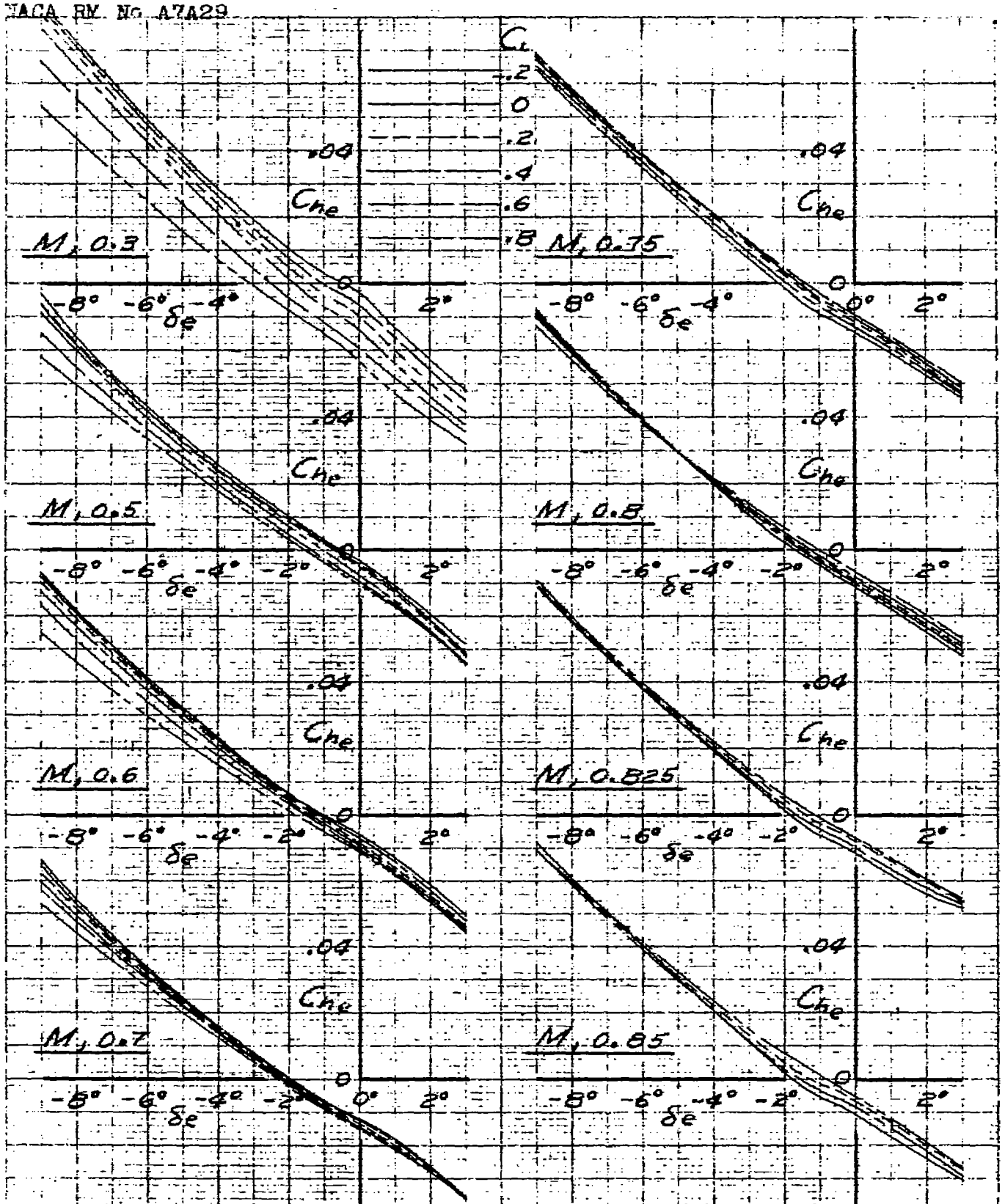

FIGURE 15.-VARIATION OF ELEVATOR HINGE-MOMENT COEFFICIENT WITH ELEVATOR ANGLE FOR THE COMPLETE 1/3-SCALE MODEL OF THE YP-80A AIRPLANE. TAB ANGLE, 0°.

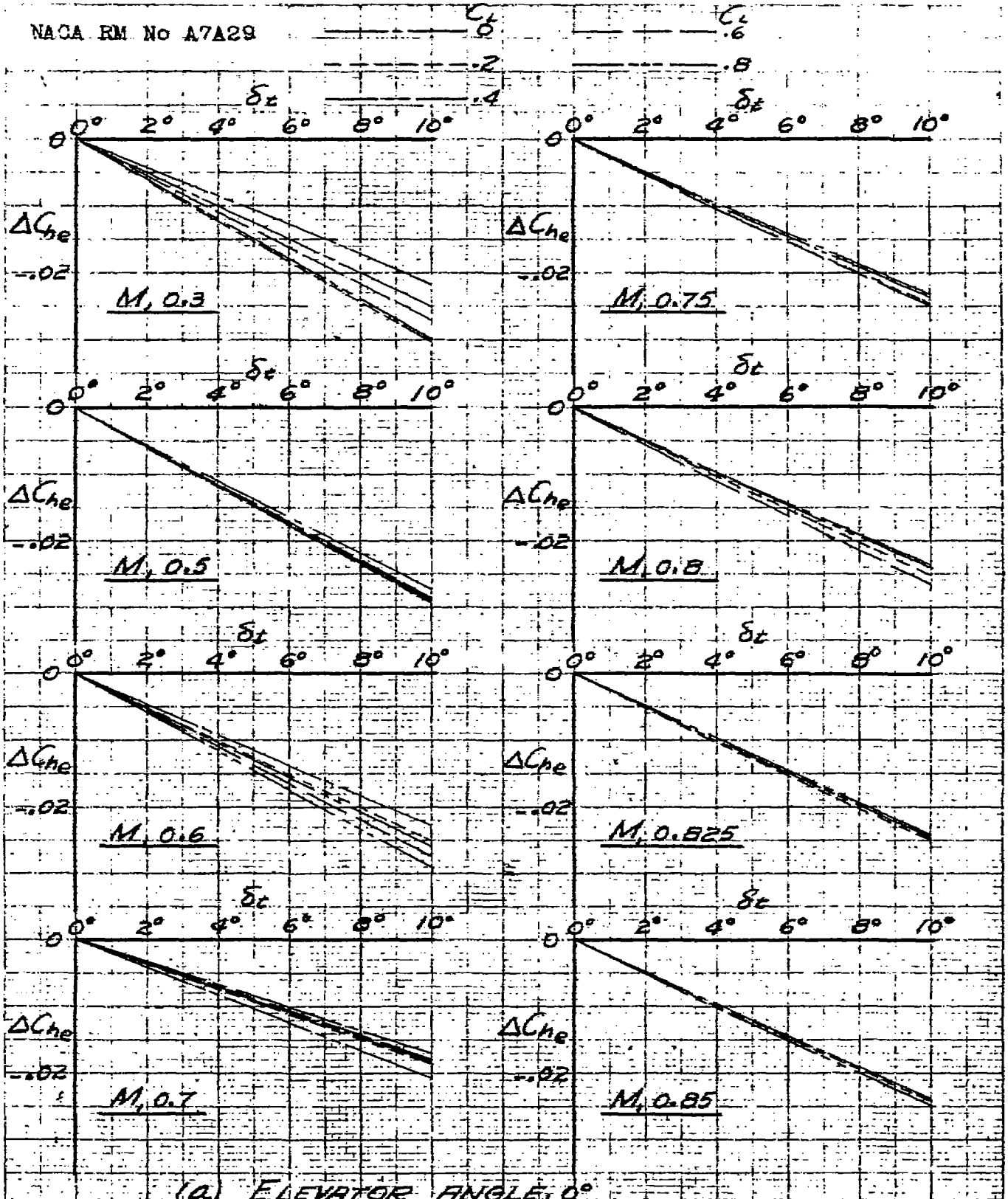

(a) ELEVATOR ANGLE, 0°

FIGURE 16.- ELEVATOR TAB EFFECTIVENESS FOR THE COMPLETE 1/3-SCALE MODEL OF THE YP-80A AIRPLANE.

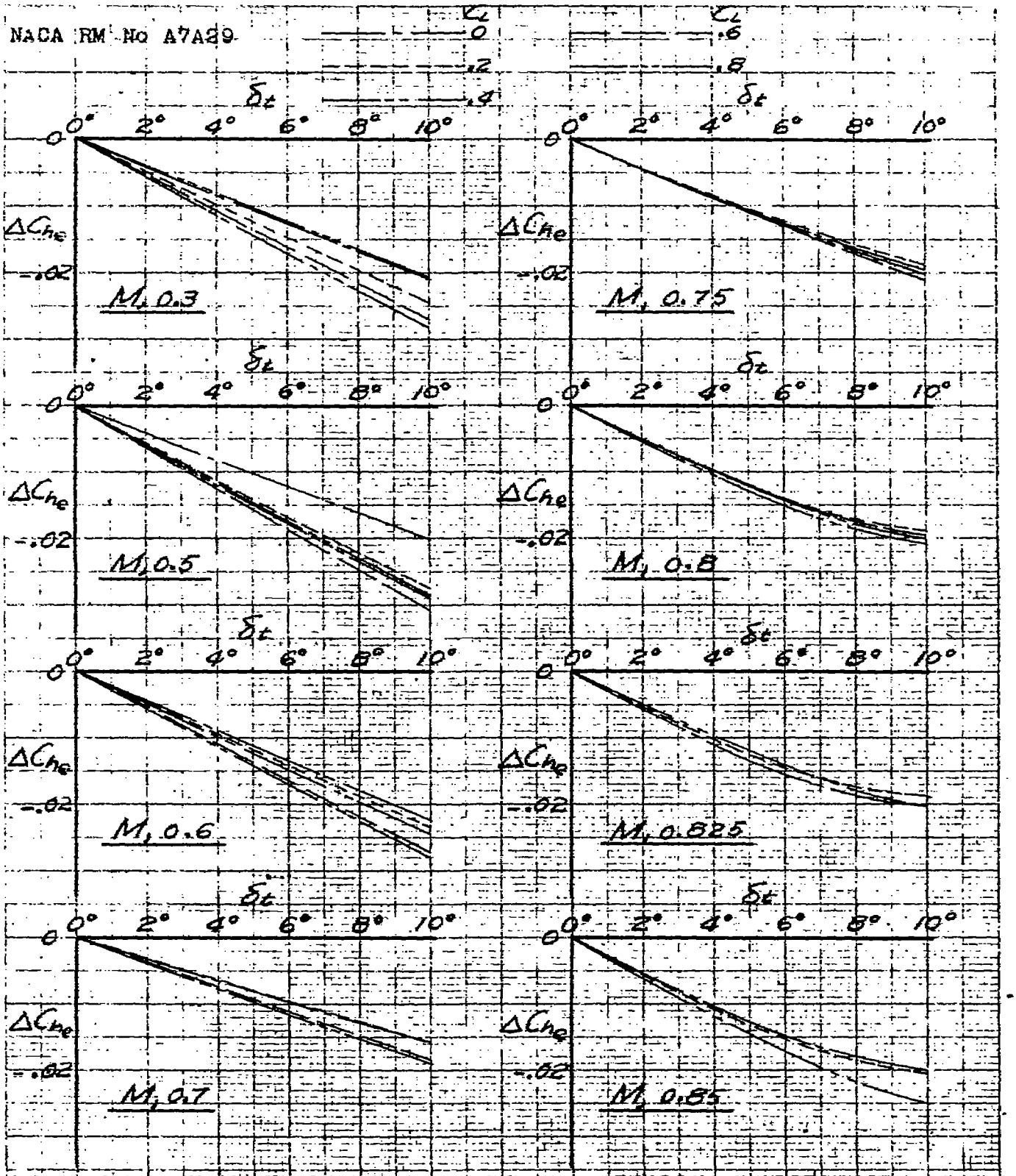

(b) ELEVATOR ANGLE, -6°

FIGURE 16.- CONCLUDED. ELEVATOR TAB EFFECTIVENESS FOR THE COMPLETE 1/3-SCALE MODEL OF THE YP-80A AIRPLANE.

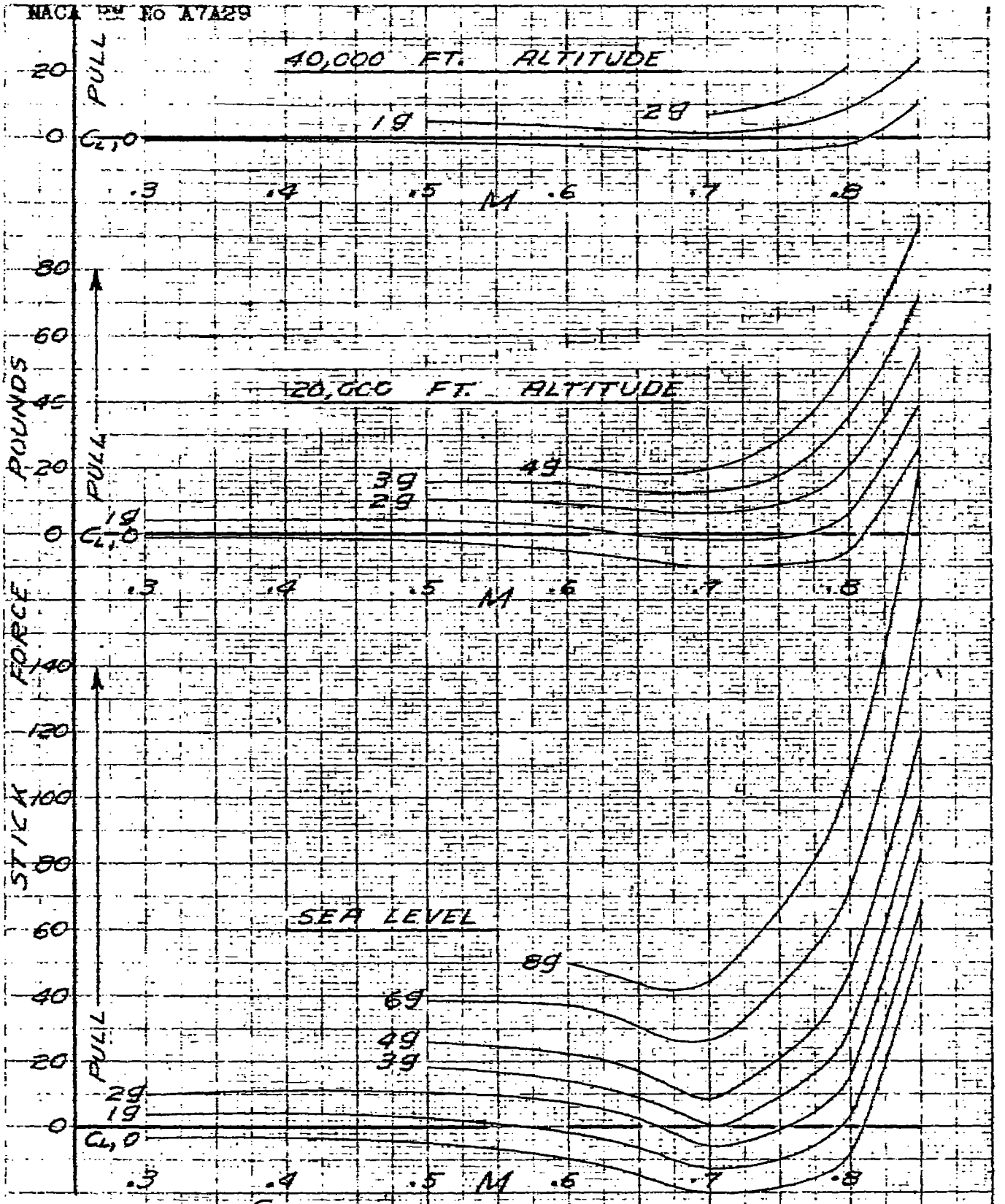

FIGURE 17.- CALCULATED STICK FORCES DURING PULL-UPS FOR THE YP-80A AIRPLANE AT THREE ALTITUDES. AIRPLANE TRIMMED AT 450 MILES PER HOUR AT 20,000 FEET ALTITUDE.

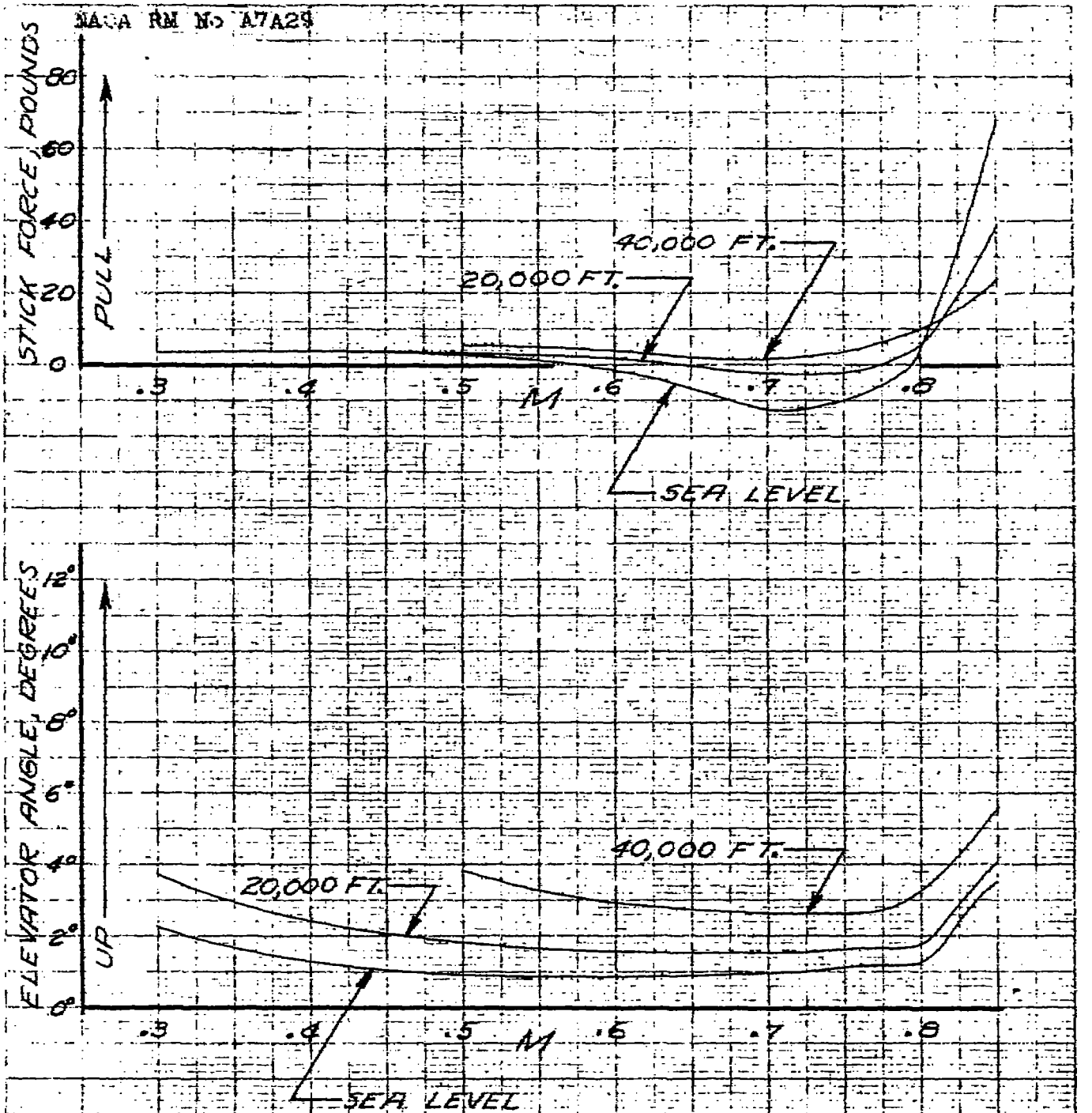

FIGURE 18.— CALCULATED STICK FORCE AND ELEVATOR ANGLE REQUIRED FOR LEVEL FLIGHT FOR THE YP-80A AIRPLANE TRIMMED AT 450 MILES PER HOUR AT 20,000 FEET ALTITUDE.

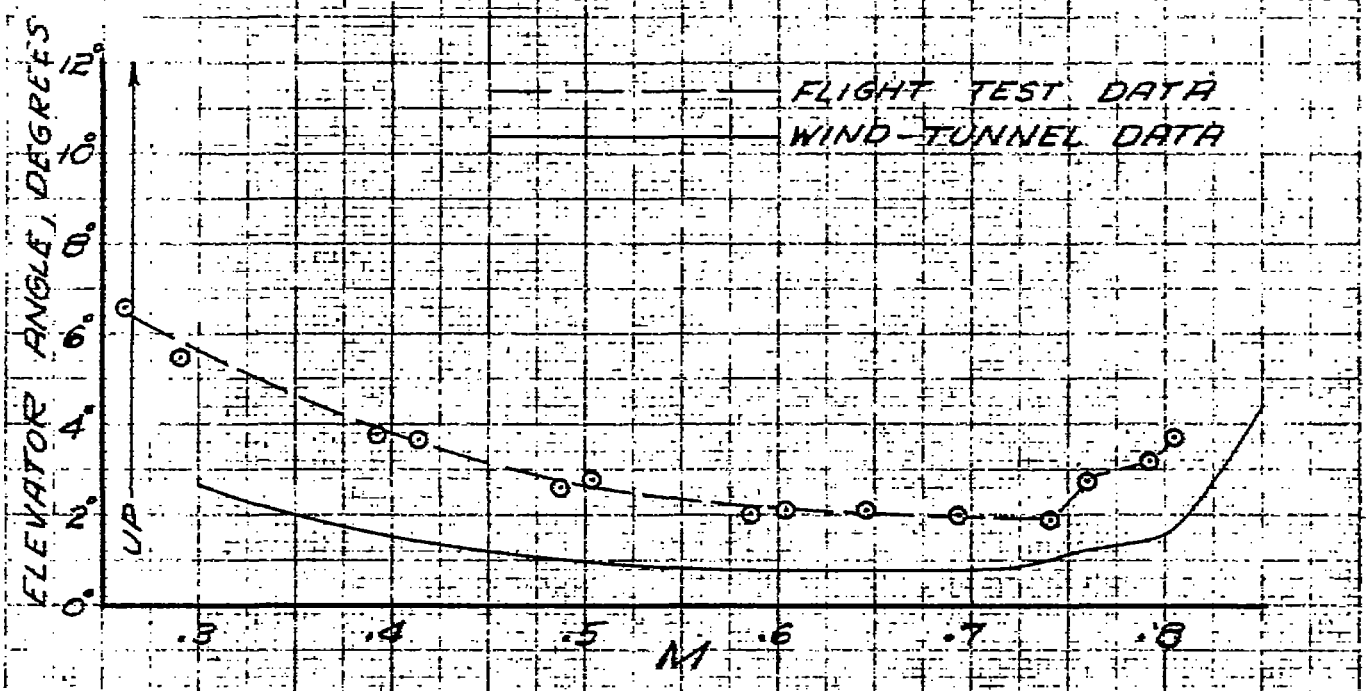

C.G. AT 28 PER CENT M.A.C.
WING LOADING 45 LB./SQ.FT.
20,000 FT. ALTITUDE

FIGURE 19.—A COMPARISON OF THE ELEVATOR ANGLE REQUIRED FOR LEVEL FLIGHT FOR THE YP-80A AIRPLANE AND THE COMPLETE 1/3-SCALE MODEL OF THE YP-80A.

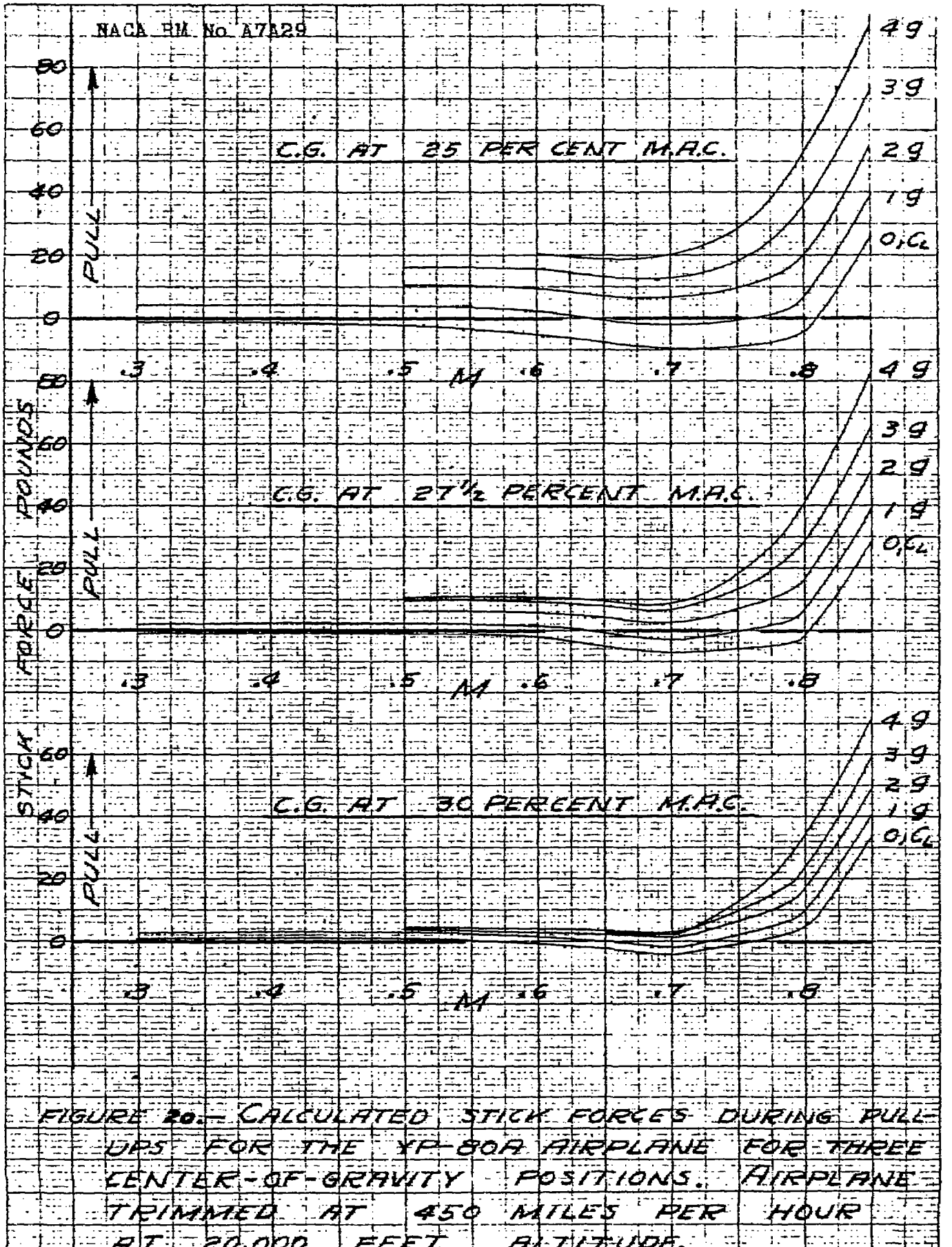

FIGURE 20.— CALCULATED STICK FORCES DURING PULL-UPS FOR THE YP-80A AIRPLANE FOR THREE CENTER-OF-GRAVITY POSITIONS. AIRPLANE TRIMMED AT 450 MILES PER HOUR AT 20,000 FEET ALTITUDE.

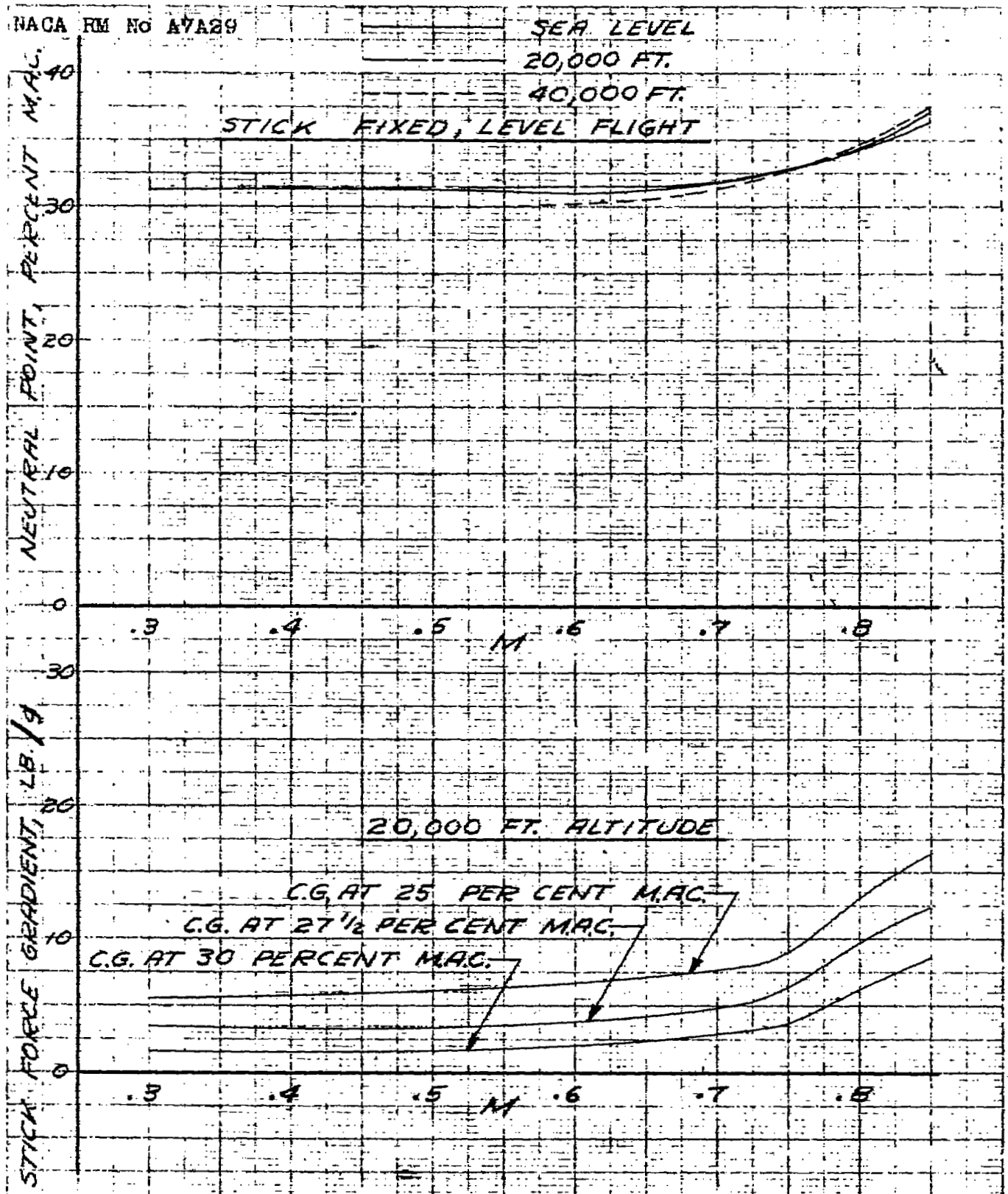

FIGURE 21.—VARIATION OF NEUTRAL POINT AND STICK FORCE GRADIENT FOR THE YP-80A AIRPLANE.

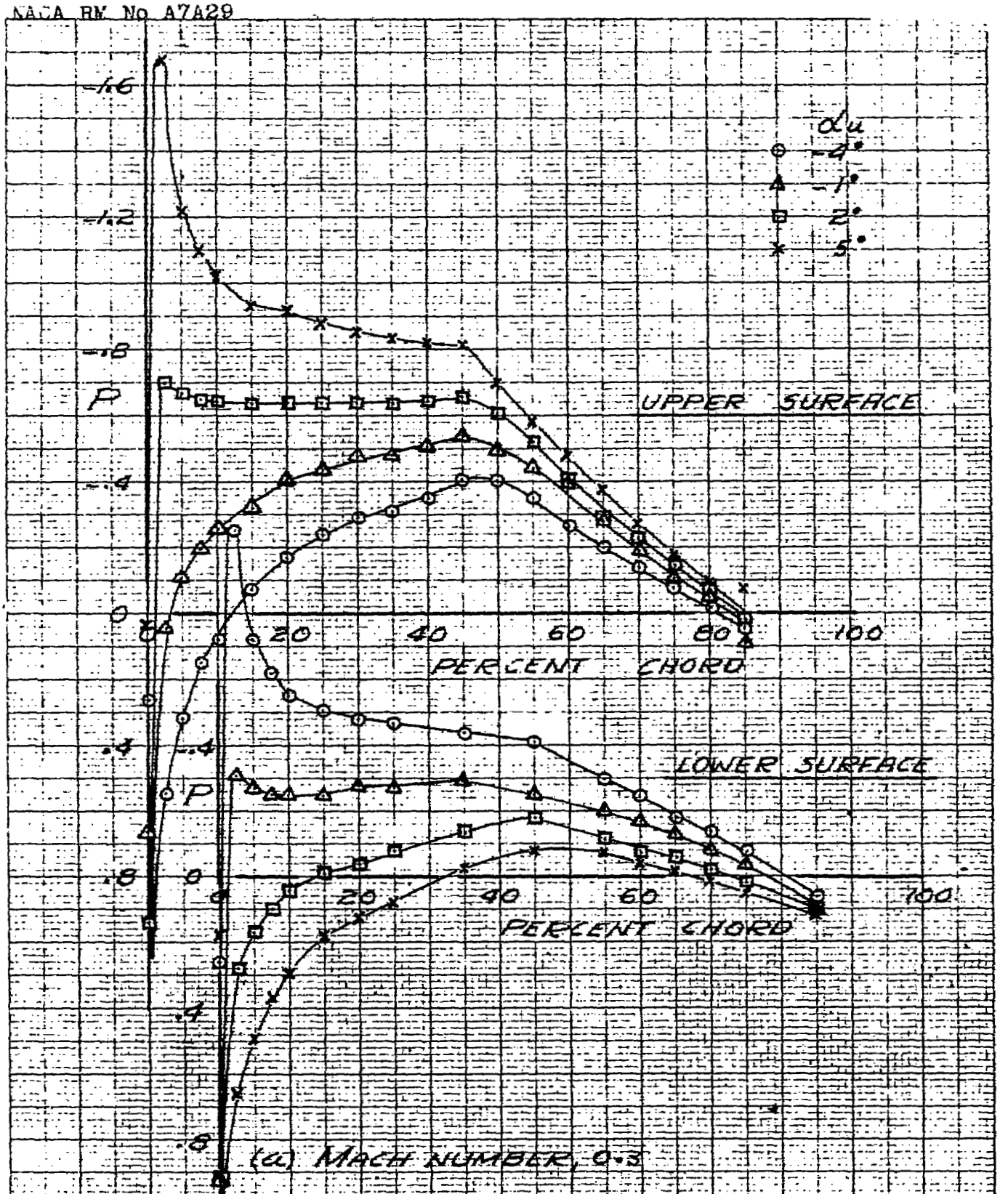

FIGURE 22.- PRESSURE DISTRIBUTION OVER THE WING OF THE COMPLETE 1/3-SCALE MODEL OF THE YP-80A AIRPLANE. WING STATION, 26.00 INCHES.

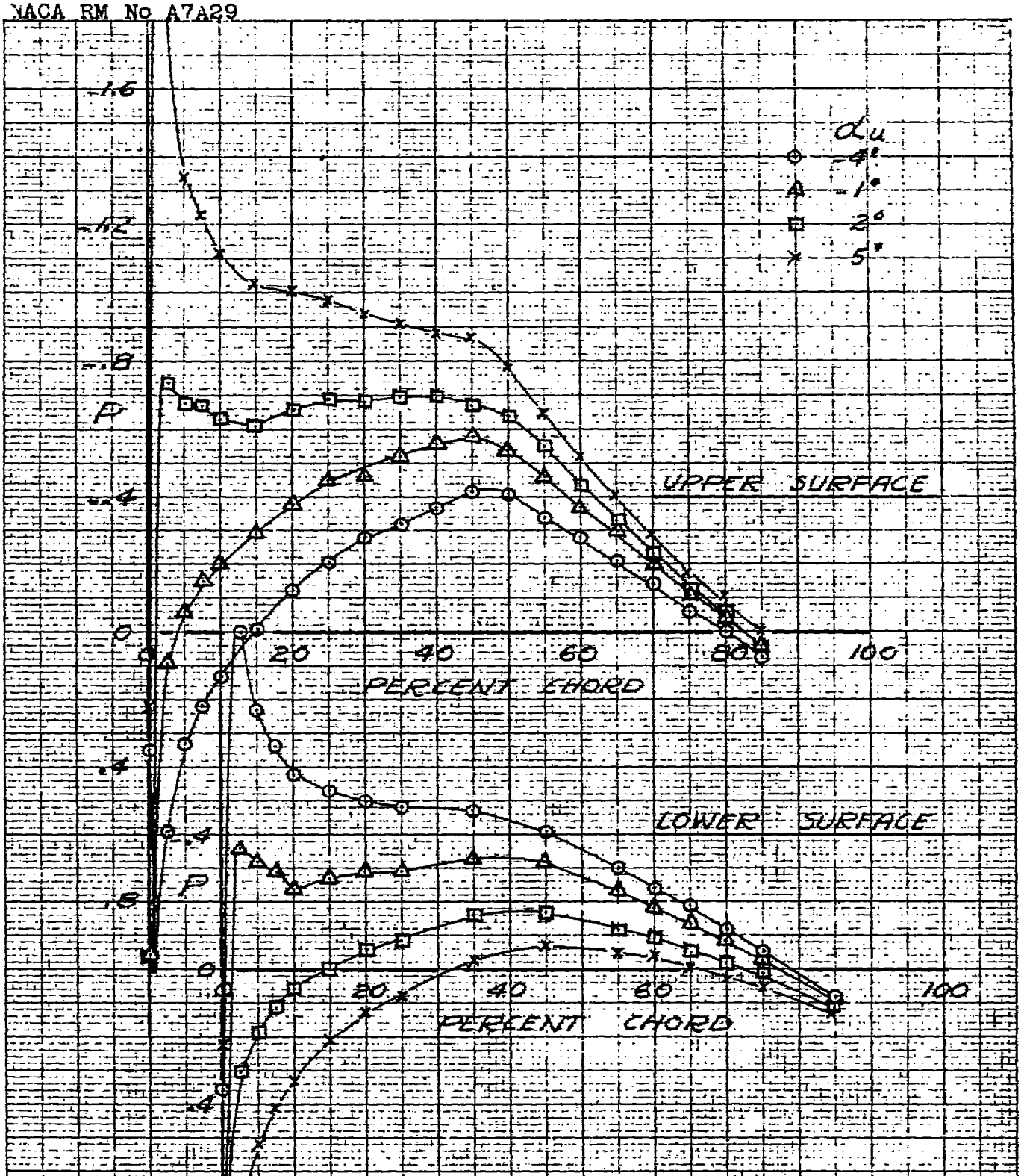

FIGURE 22.- CONTINUED. PRESSURE DISTRIBUTION OVER THE WING OF THE COMPLETE 1/3-SCALE MODEL OF THE YP-80A AIRPLANE. WING STATION, 26.00 INCHES.

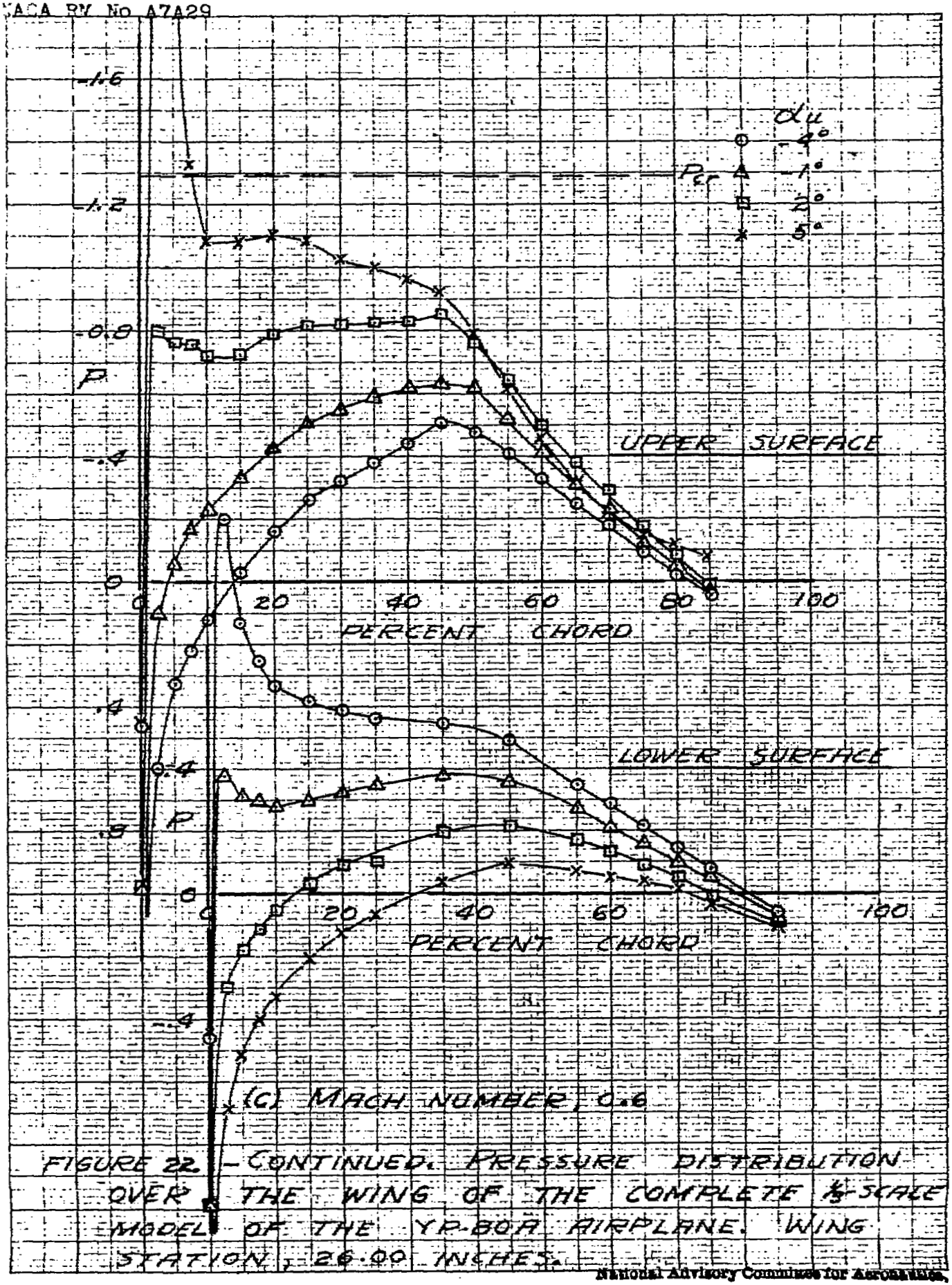

(c) MACH NUMBER, 0.6

FIGURE 22.- CONTINUED. PRESSURE DISTRIBUTION OVER THE WING OF THE COMPLETE ¼-SCALE MODEL OF THE YP-80A AIRPLANE. WING STATION, 26.00 INCHES.

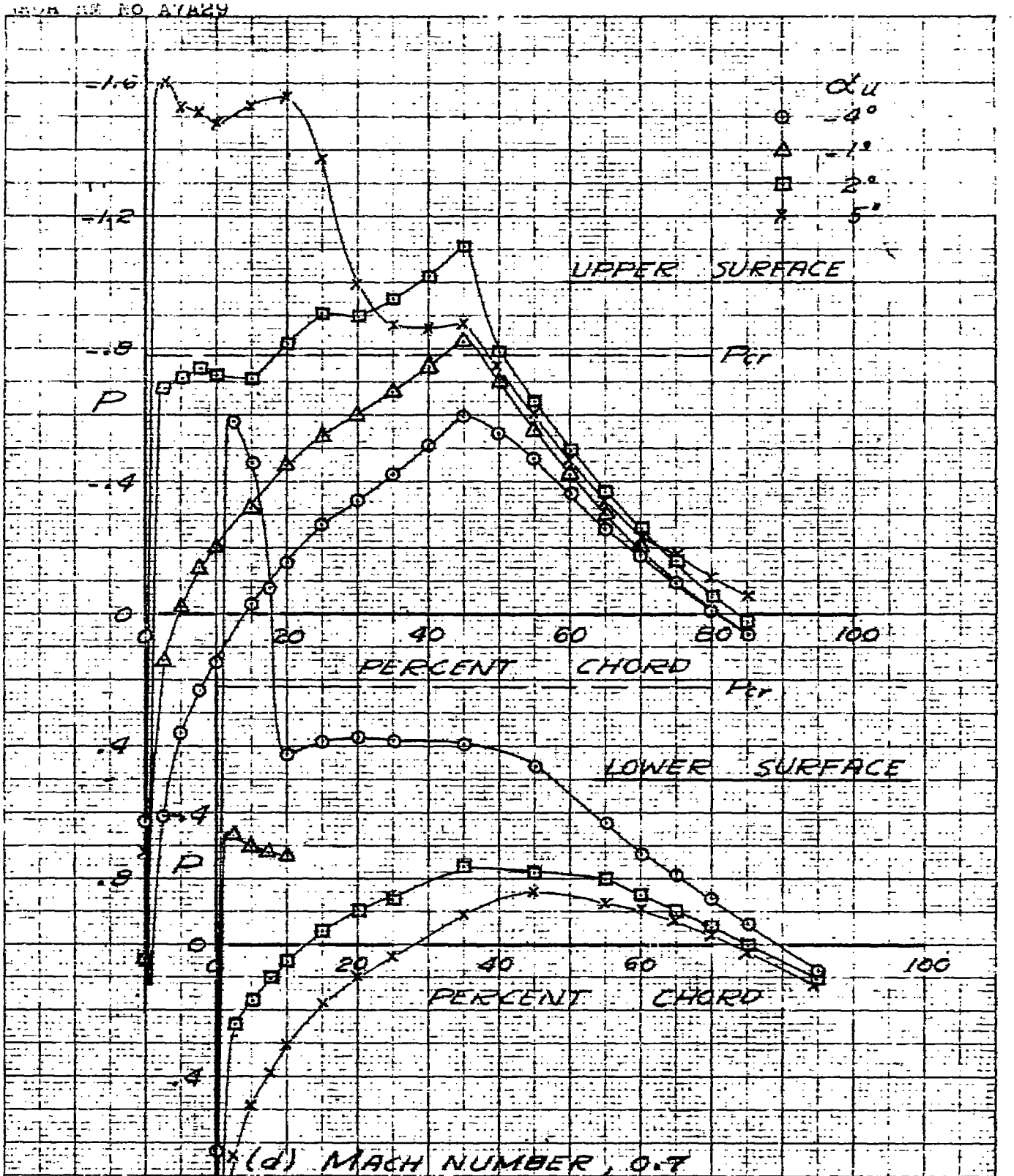

(d) MACH NUMBER, 0.7

FIGURE 22.—CONTINUED. PRESSURE DISTRIBUTION OVER THE WING OF THE COMPLETE 1/3-SCALE MODEL OF THE YP-80A AIRPLANE. WING STATION 26.00 INCHES.

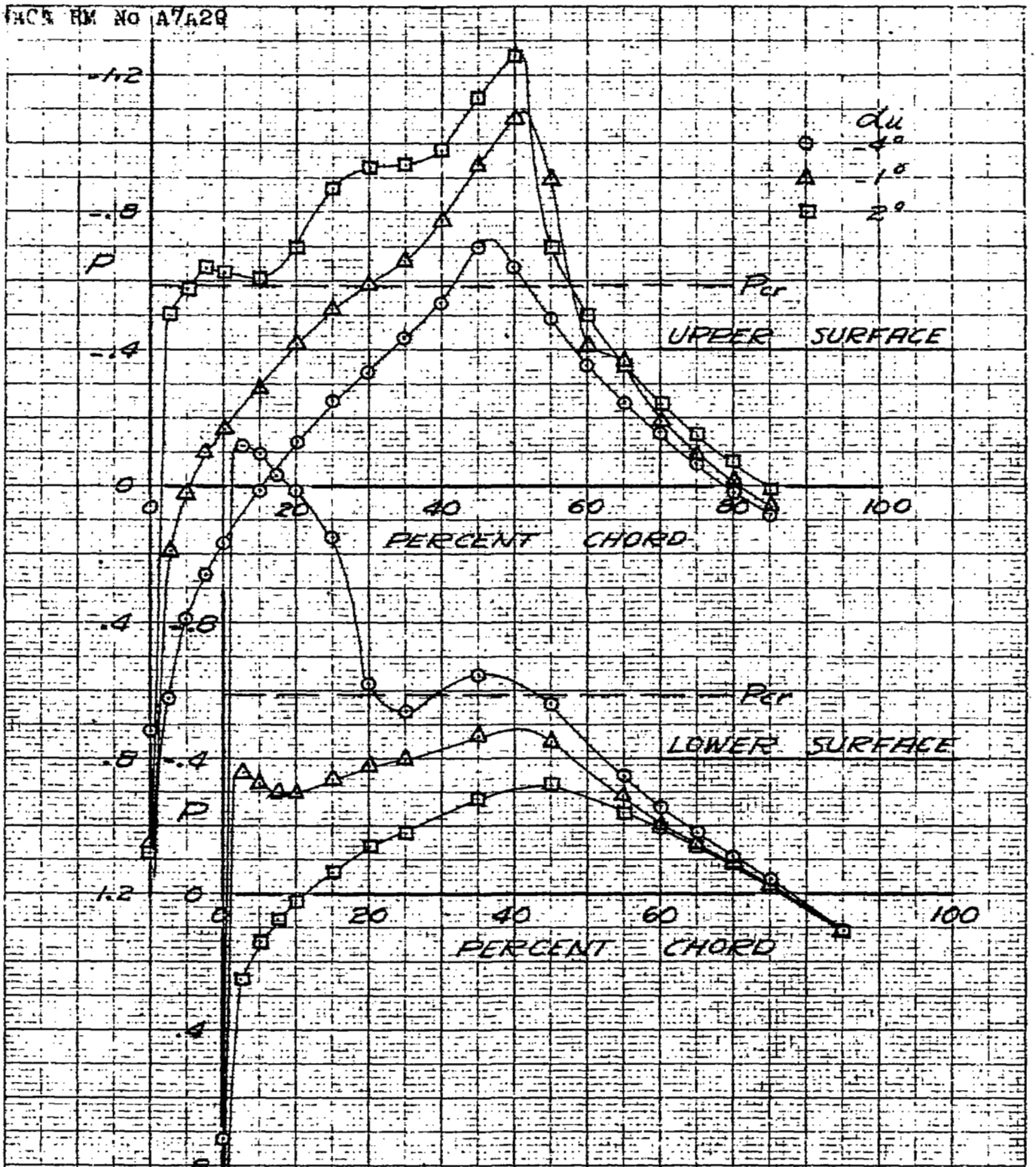

(e) MACH NUMBER, 0.75

FIGURE 22.- CONTINUED. PRESSURE DISTRIBUTION OVER THE WING OF THE COMPLETE 1/3-SCALE MODEL OF THE YP-80A AIRPLANE. WING STATION, 26.00 INCHES.

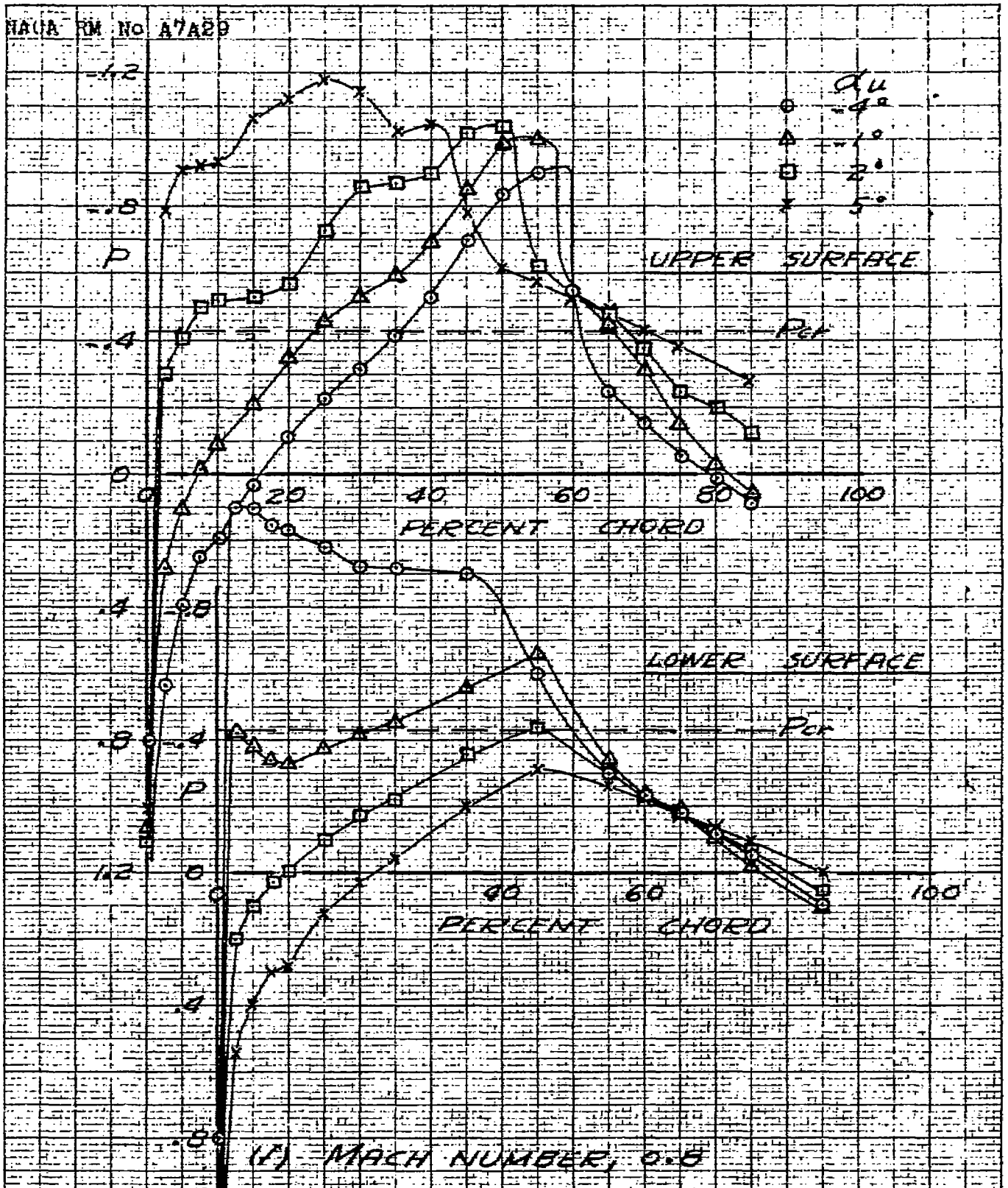

(f) MACH NUMBER, 0.8

FIGURE 22.—CONTINUED. PRESSURE DISTRIBUTION OVER THE WING OF THE COMPLETE ½-SCALE MODEL OF THE YP-80A AIRPLANE. WING STATION, 26.00 INCHES.

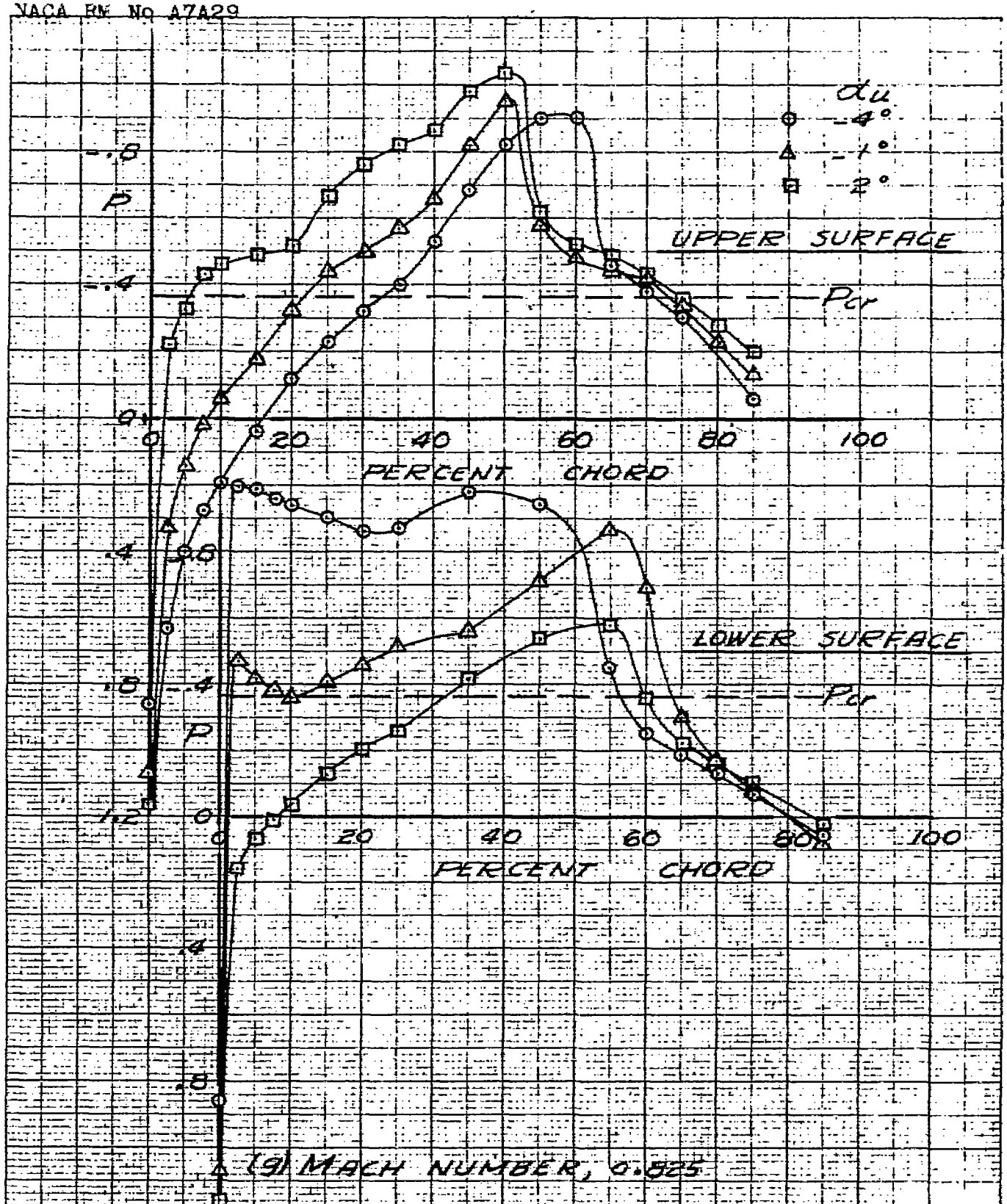

FIGURE 22.- CONTINUED. PRESSURE DISTRIBUTION OVER THE WING OF THE COMPLETE ⅛-SCALE MODEL OF THE YP-80A AIRPLANE. WING STATION, 26.00 INCHES.

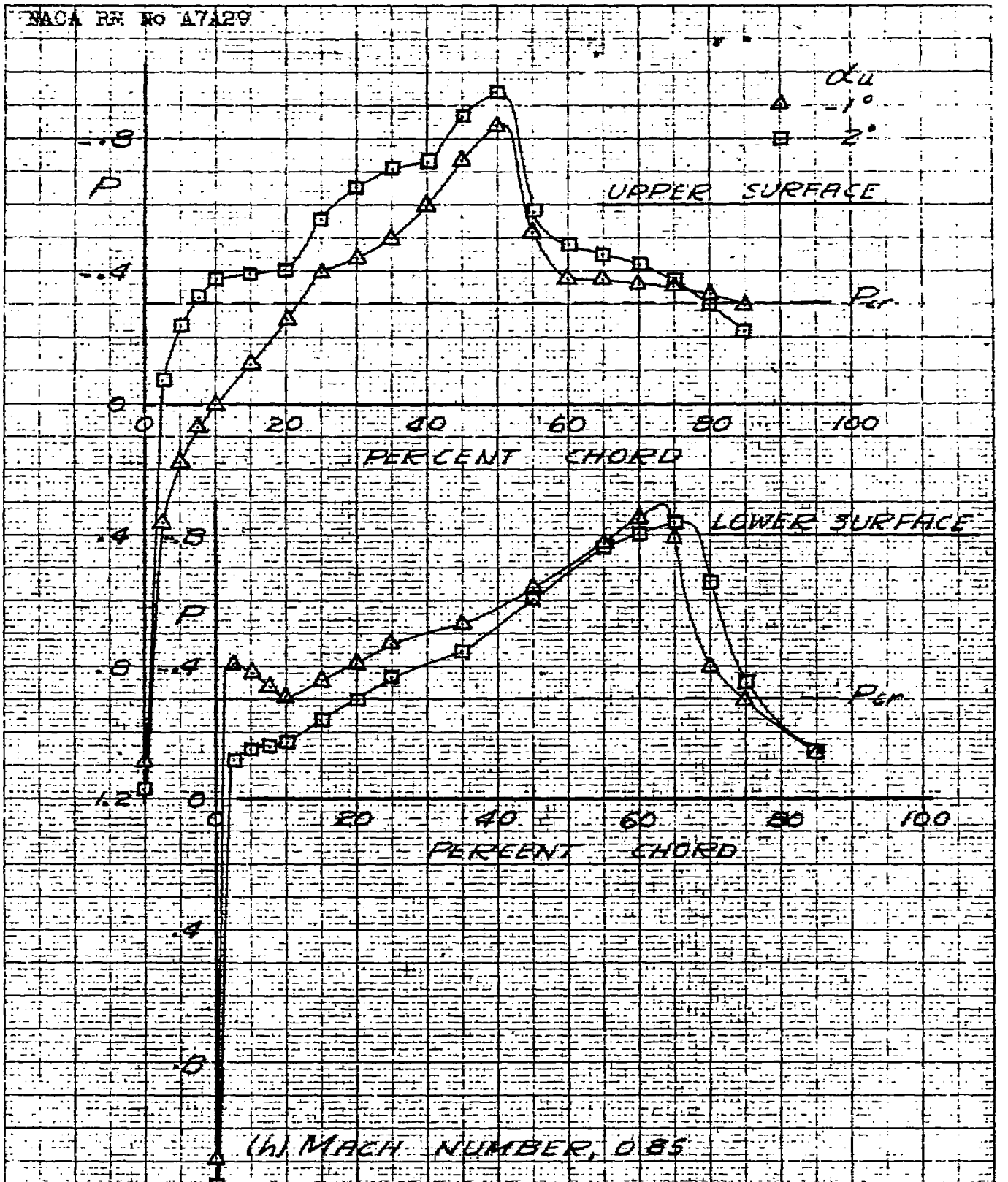

(h) MACH NUMBER, 0.85

FIGURE 22.- CONCLUDED. PRESSURE DISTRIBUTION OVER THE WING OF THE COMPLETE 1/3-SCALE MODEL OF THE YP-80A AIRPLANE. WING STATION, 26.00 INCHES.

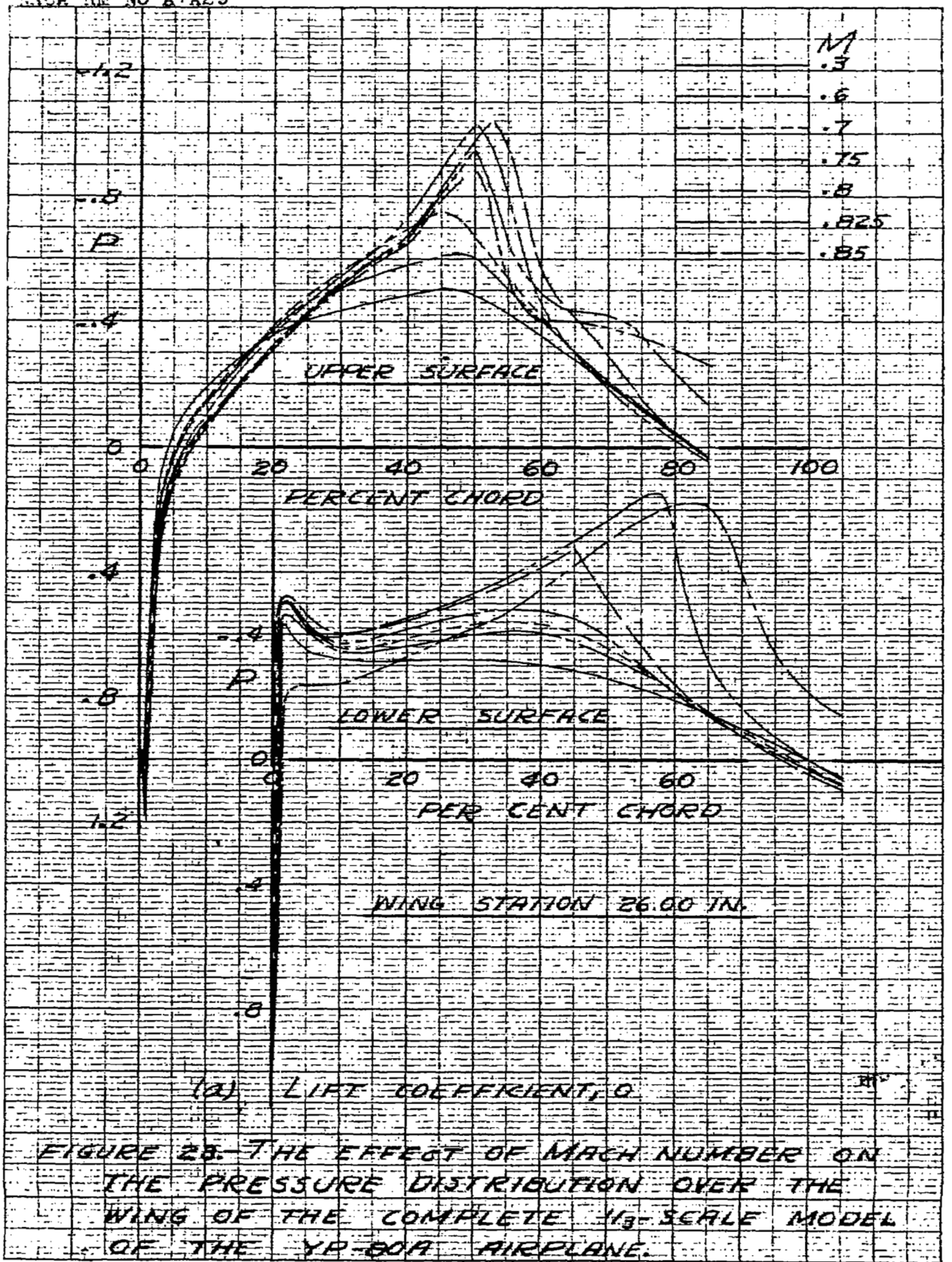

(a) LIFT COEFFICIENT, 0

FIGURE 28.- THE EFFECT OF MACH NUMBER ON THE PRESSURE DISTRIBUTION OVER THE WING OF THE COMPLETE 1/3-SCALE MODEL OF THE YP-80A AIRPLANE.

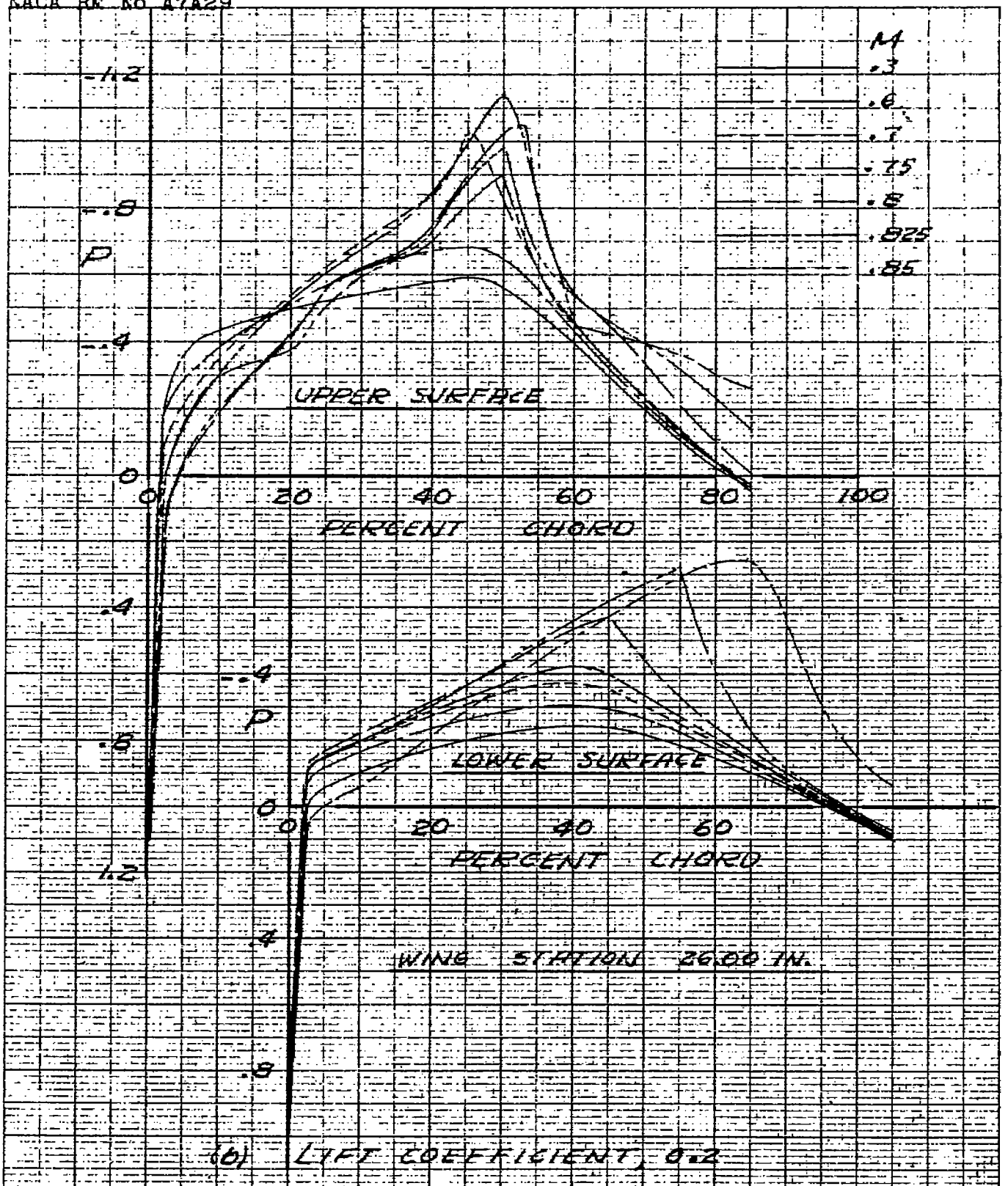

(b) LIFT COEFFICIENT, 0.2

FIGURE 23.- CONCLUDED. THE EFFECT OF MACH NUMBER ON THE PRESSURE DISTRIBUTION OVER THE WING OF THE COMPLETE 1/3-SCALE MODEL OF THE YP-60A AIRPLANE.

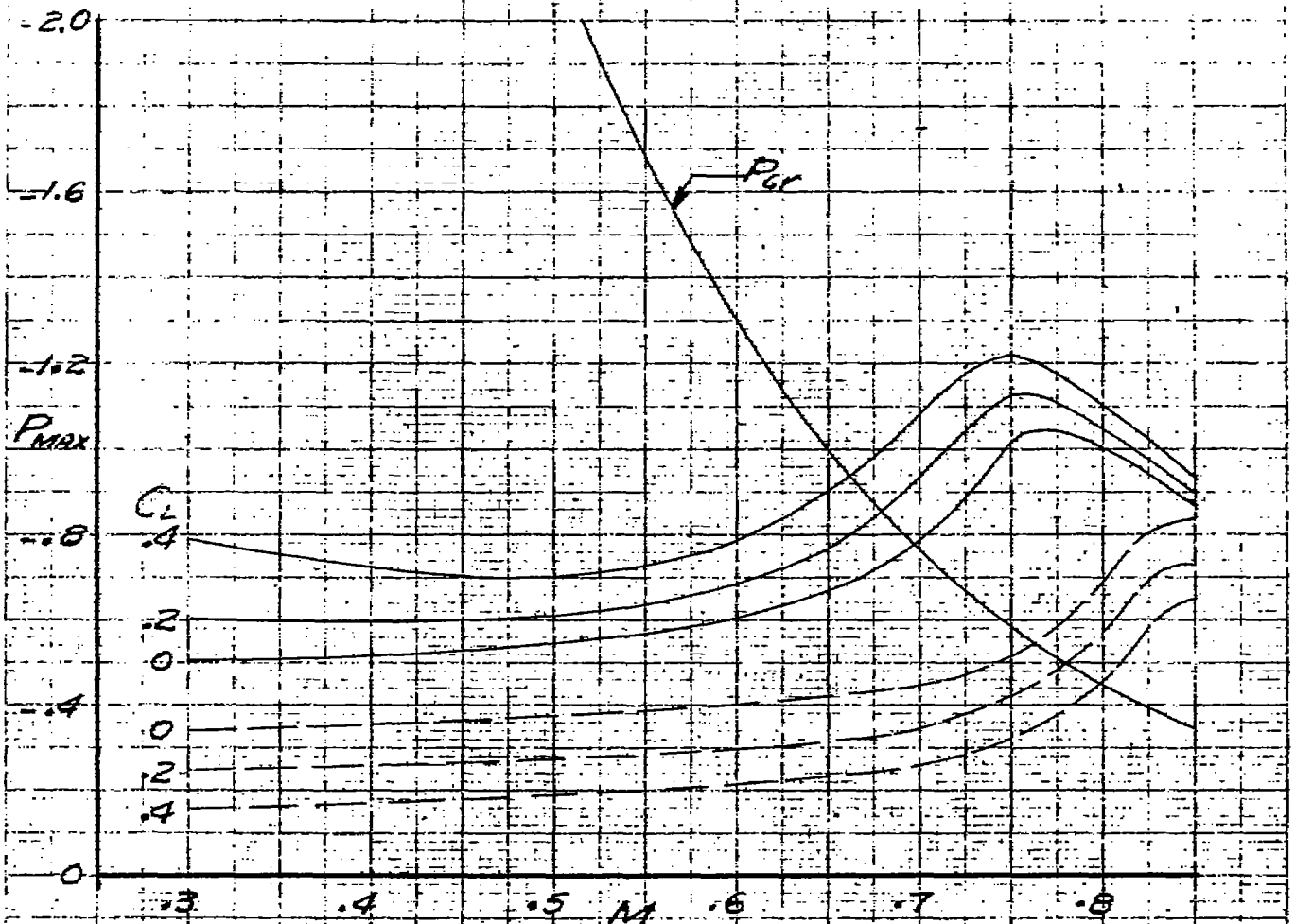

FIGURE 24.—THE VARIATION OF MAXIMUM PRESSURE COEFFICIENT WITH MACH NUMBER FOR THE COMPLETE 1/3-SCALE MODEL OF THE YP-80A AIRPLANE. WING STATION, 26.00 INCHES

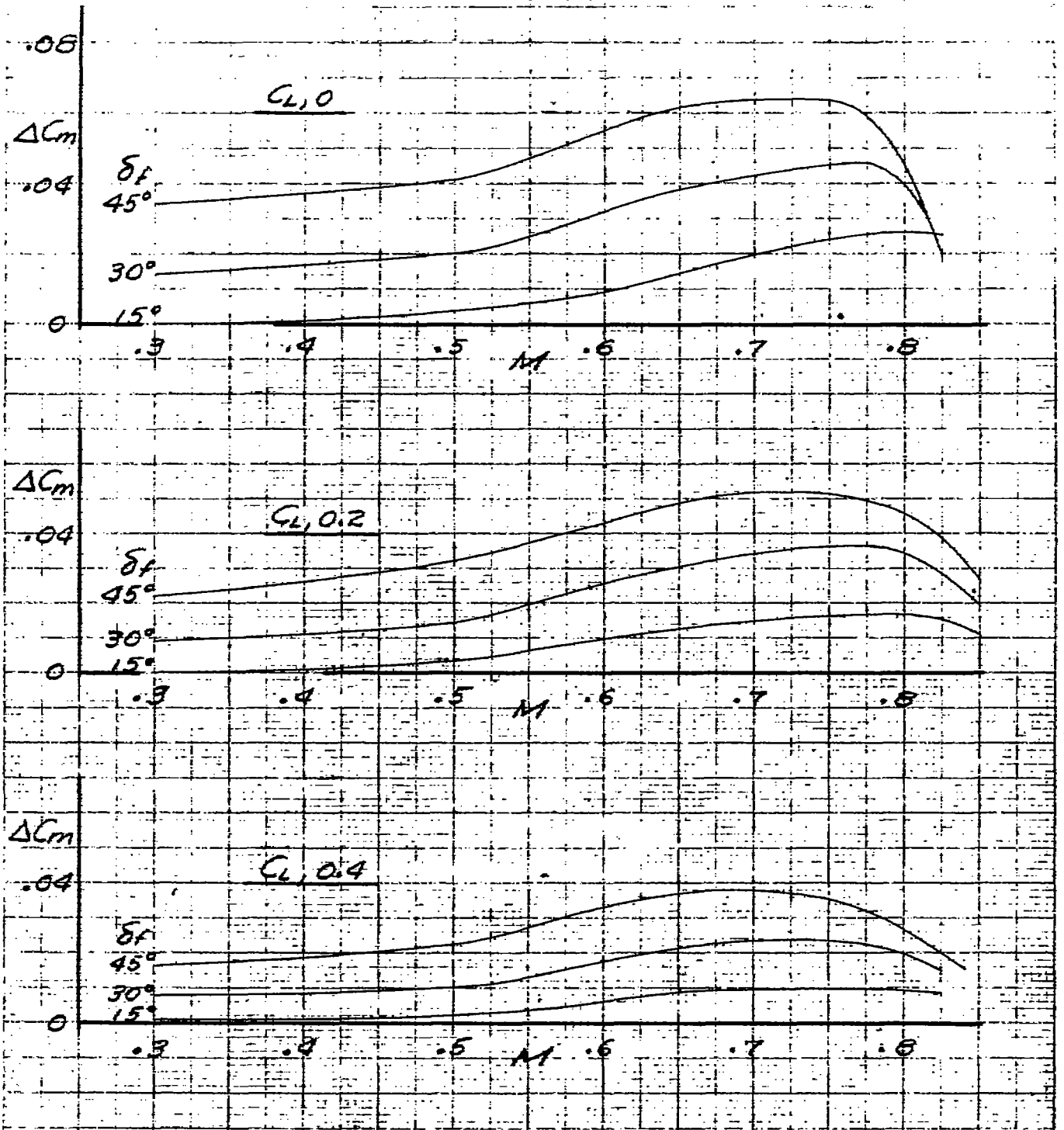

FIGURE 25.—THE INCREMENT OF PITCHING-MOMENT COEFFICIENT FROM THE WING DIVE-RECOVERY FLAPS FOR THE COMPLETE V_3-SCALE MODEL OF THE YP-80A AIRPLANE. FLAP POSITION, 35 PERCENT OF THE M.A.C.

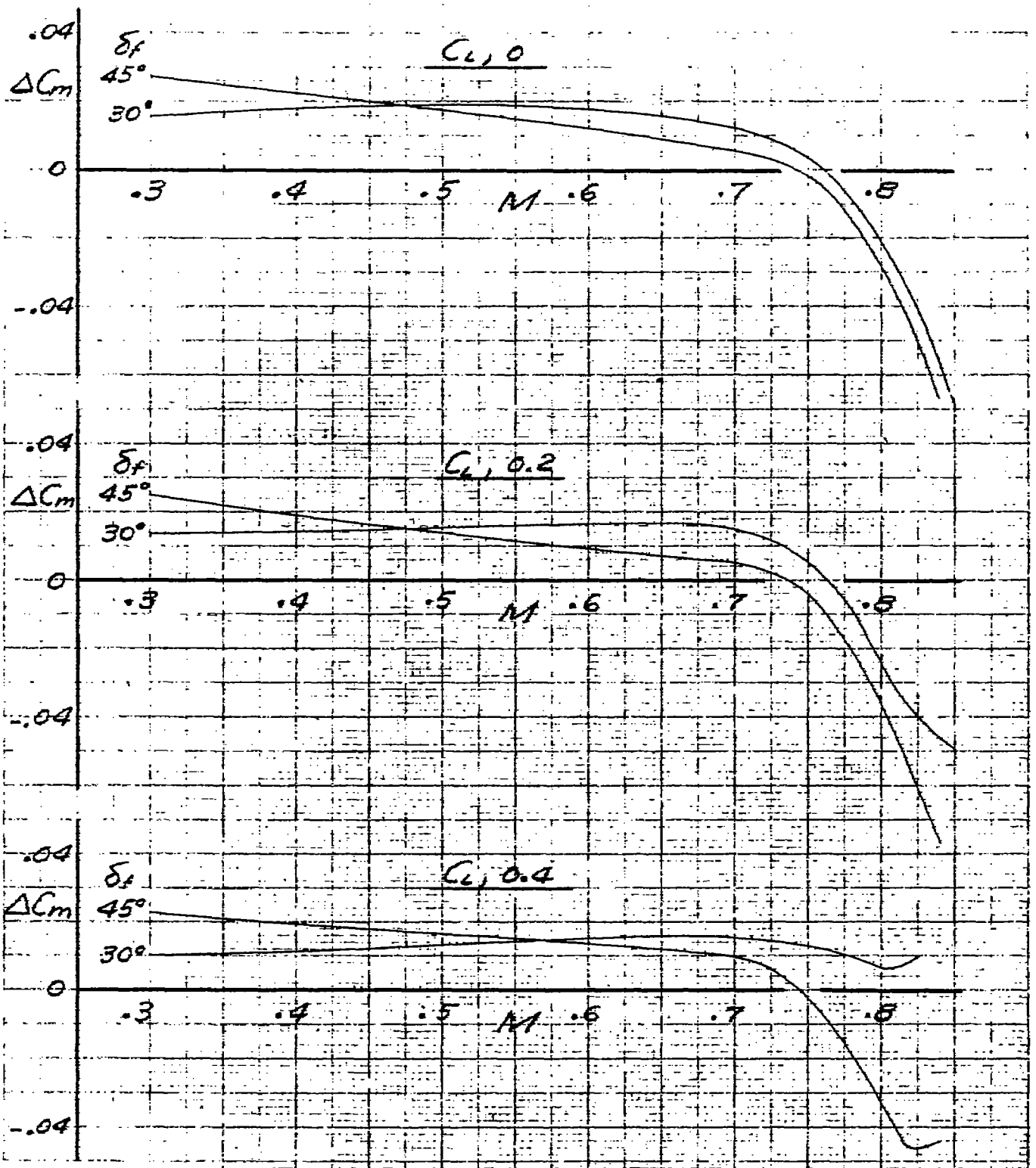

FIGURE 26.—THE INCREMENT OF PITCHING-MOMENT COEFFICIENT FROM THE WING DIVE-RECOVERY FLAPS FOR THE 1/3-SCALE MODEL OF THE YP-80A AIRPLANE LESS THE TAIL. FLAP POSITION, 35 PERCENT OF THE M.A.C.

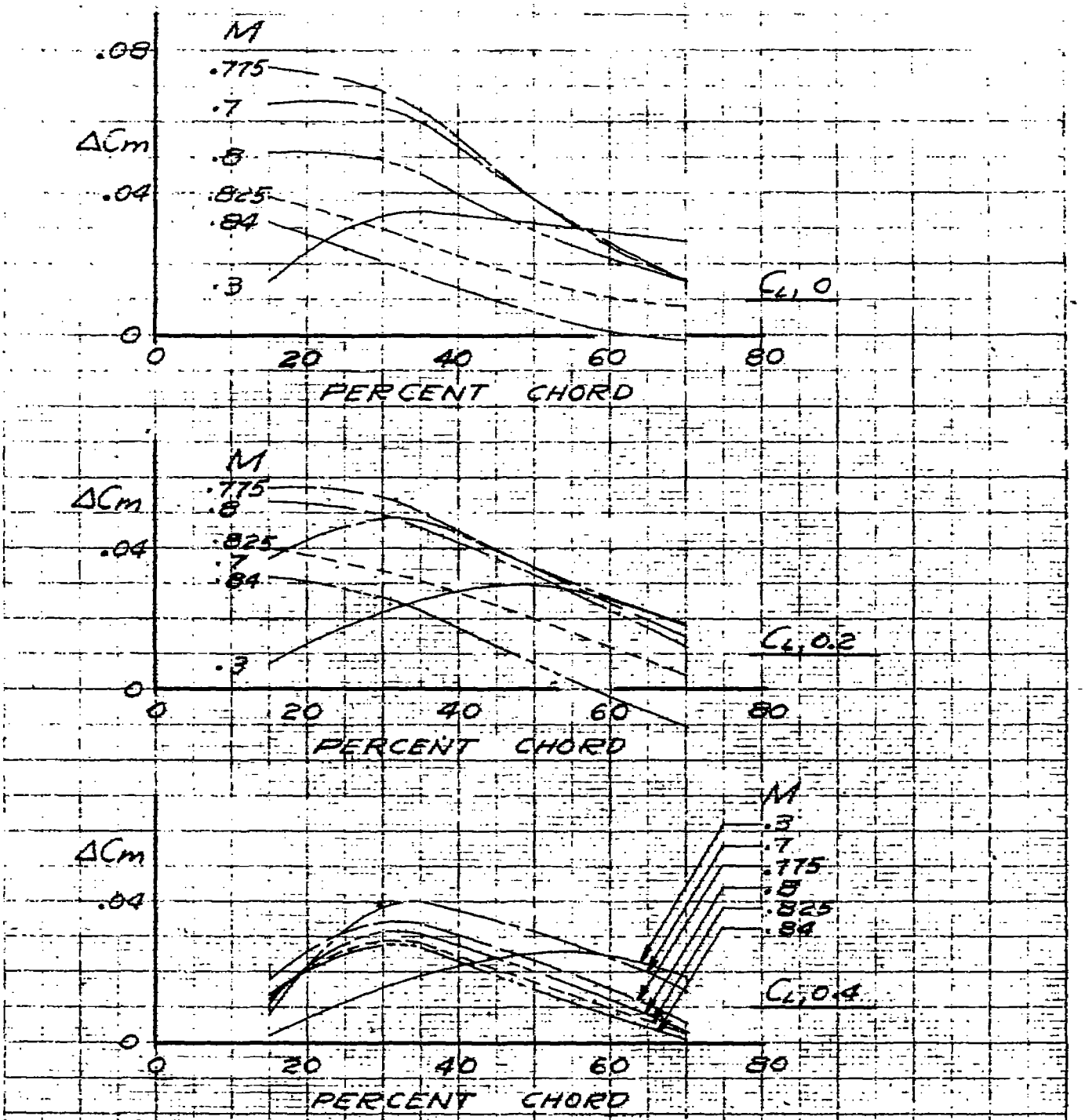

FIGURE 27.-THE EFFECT OF FLAP LOCATION ON THE INCREMENT OF PITCHING-MOMENT COEFFICIENT FROM THE WING DIVE-RECOVERY FLAPS FOR THE COMPLETE 1/3-SCALE MODEL OF THE YP-80A AIRPLANE. FLAP ANGLE, 45°.

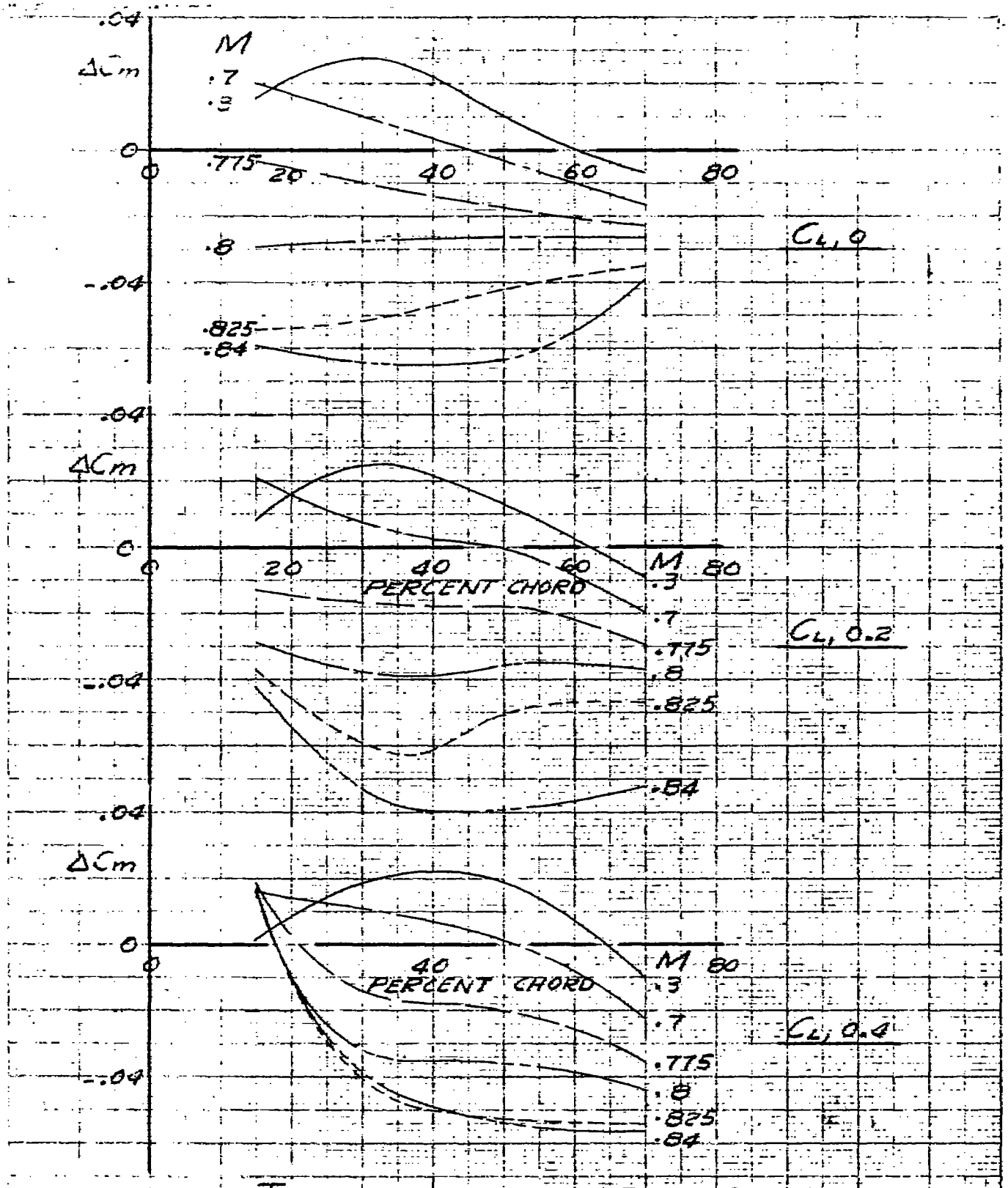

FIGURE 28.—THE EFFECT OF FLAP LOCATION ON THE INCREMENT OF PITCHING-MOMENT COEFFICIENT FROM THE WING DIVE-RECOVERY FLAPS FOR THE COMPLETE 1/3-SCALE MODEL OF THE YP-80A AIRPLANE LESS THE TAIL. FLAP ANGLE, 45°.

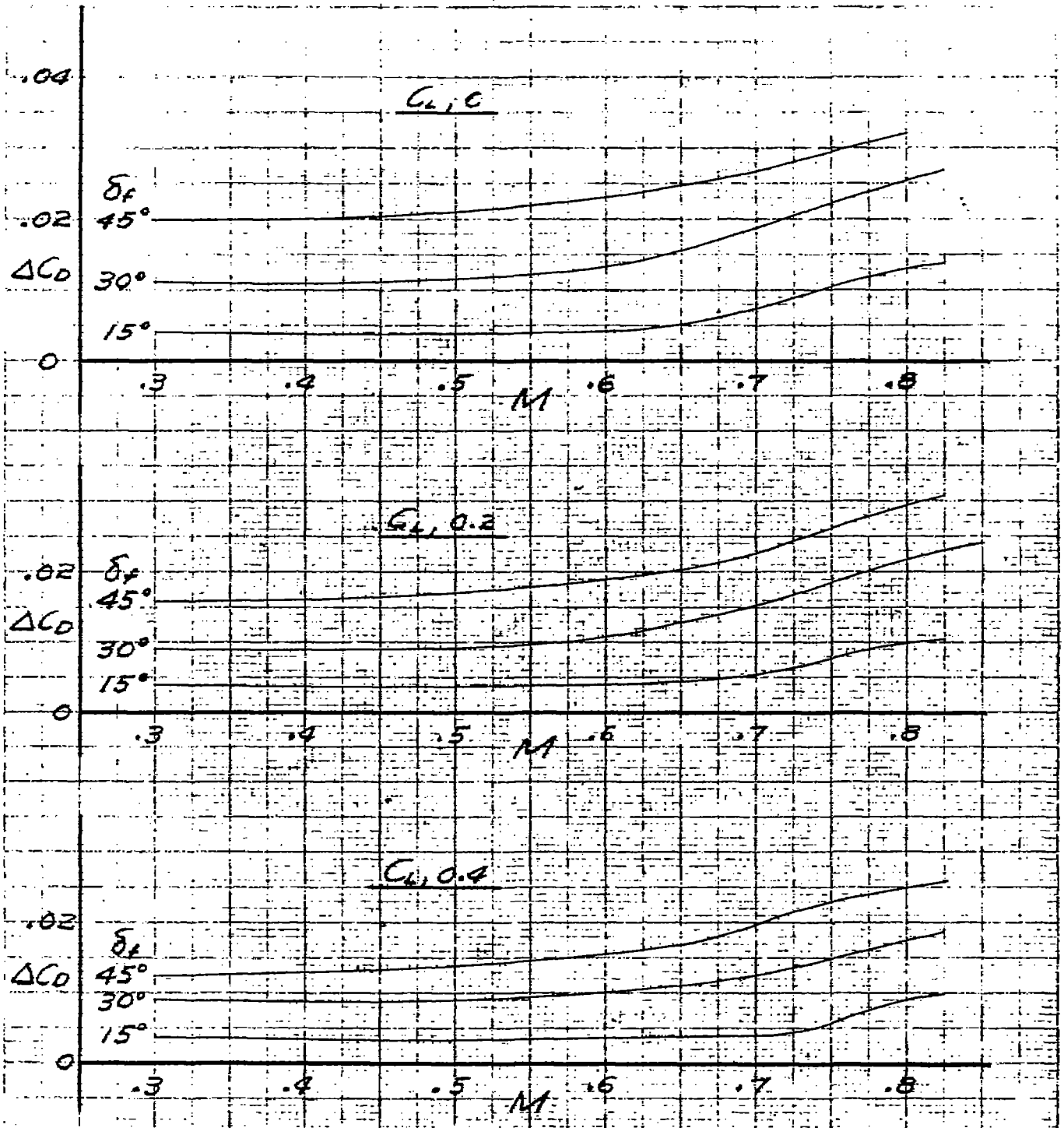

FIGURE 29.—THE INCREMENT OF DRAG COEFFICIENT FROM THE WING DIVE-RECOVERY FLAPS FOR THE COMPLETE 1/3-SCALE MODEL OF THE YP-80A AIRPLANE.

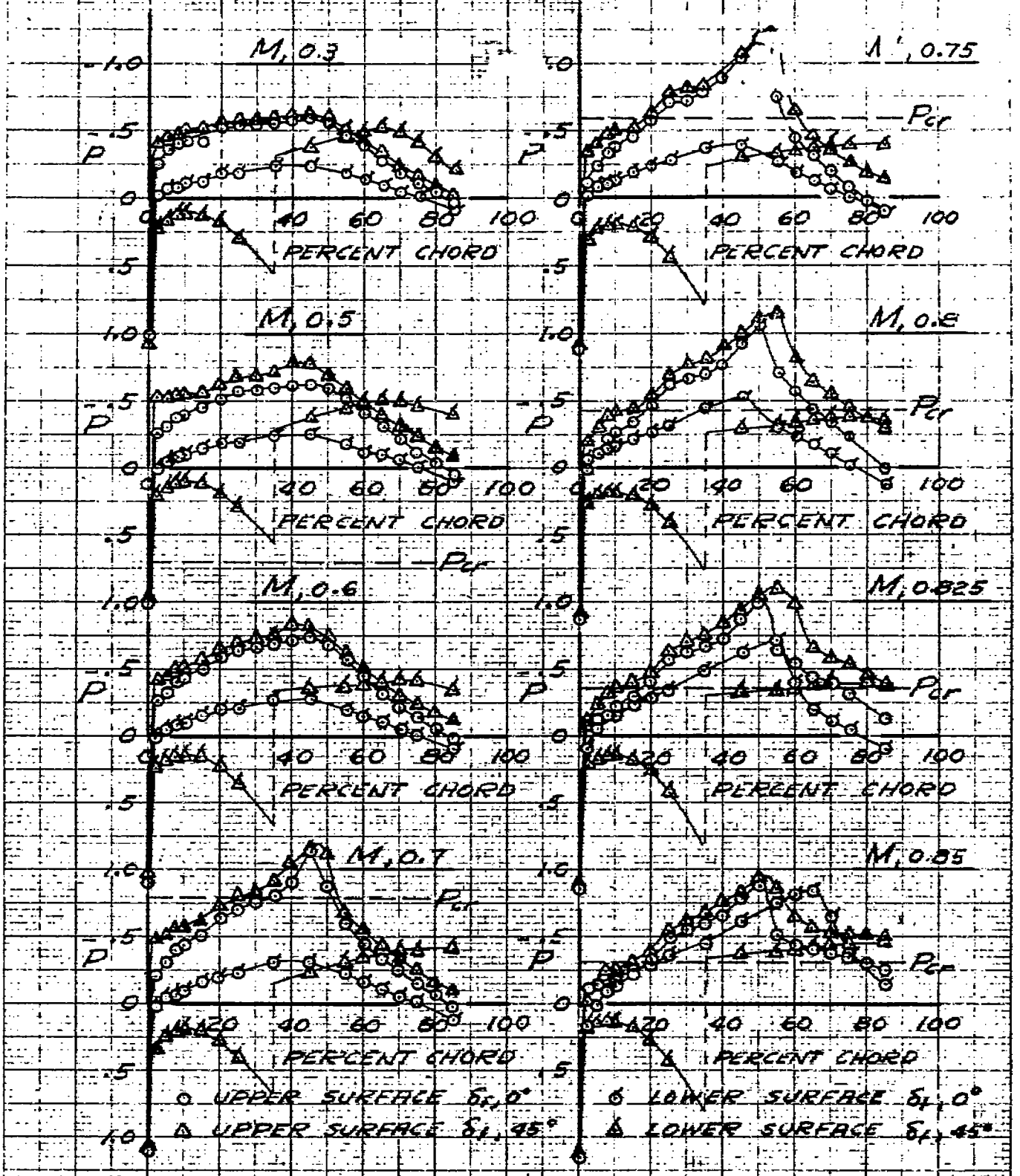

FIGURE 30.—THE EFFECT OF WING DIVE-RECOVERY FLAPS ON THE PRESSURE DISTRIBUTION OVER THE WING OF THE COMPLETE ½-SCALE MODEL OF THE YP-80A AIRPLANE. WING STATION, 26.00 INCHES; α_u, ½°.

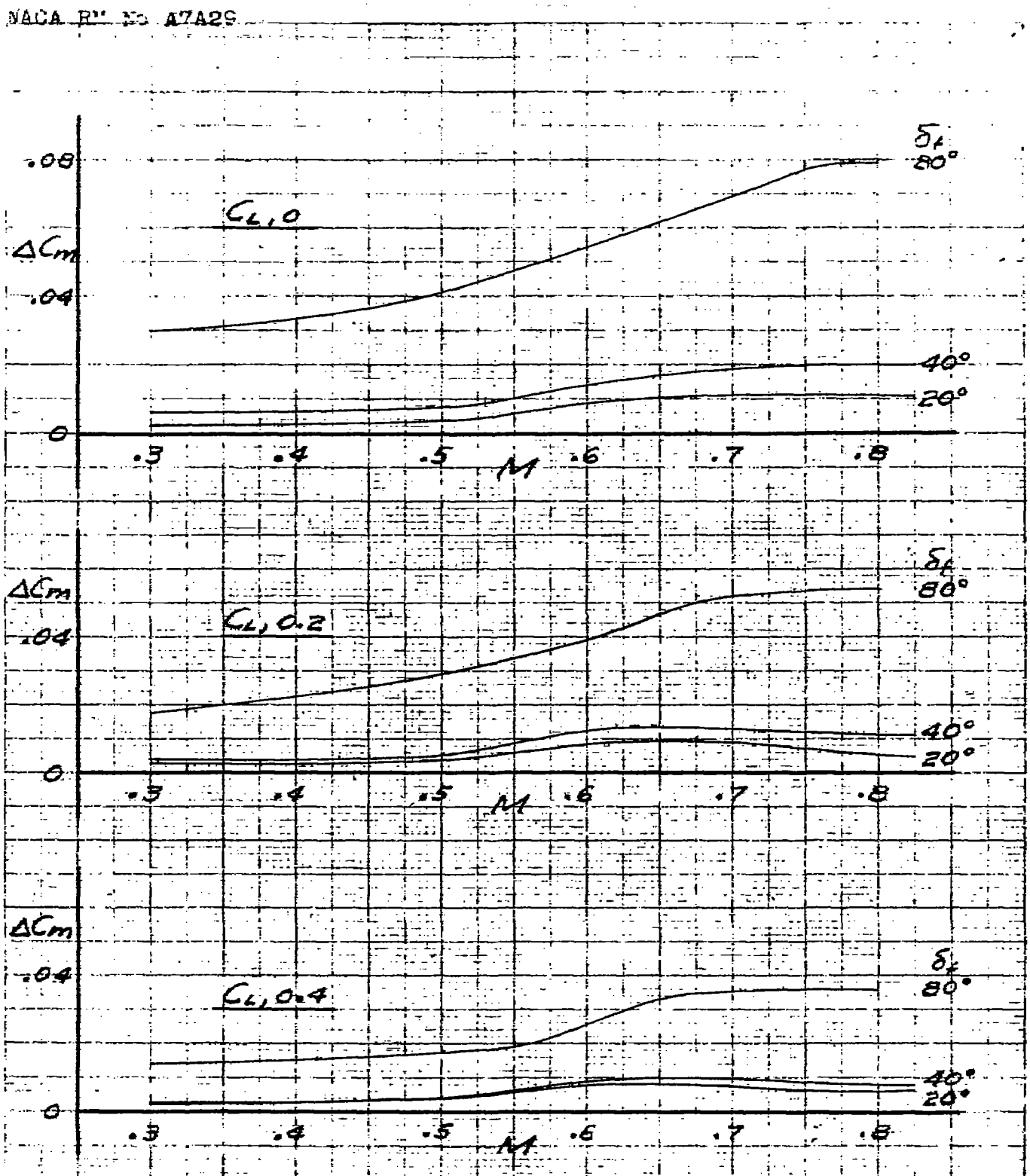

FIGURE 31.- THE INCREMENT OF PITCHING-MOMENT COEFFICIENT FROM THE FUSELAGE DIVE-RECOVERY FLAPS FOR THE COMPLETE 1/3-SCALE MODEL OF THE YP-80A AIRPLANE.

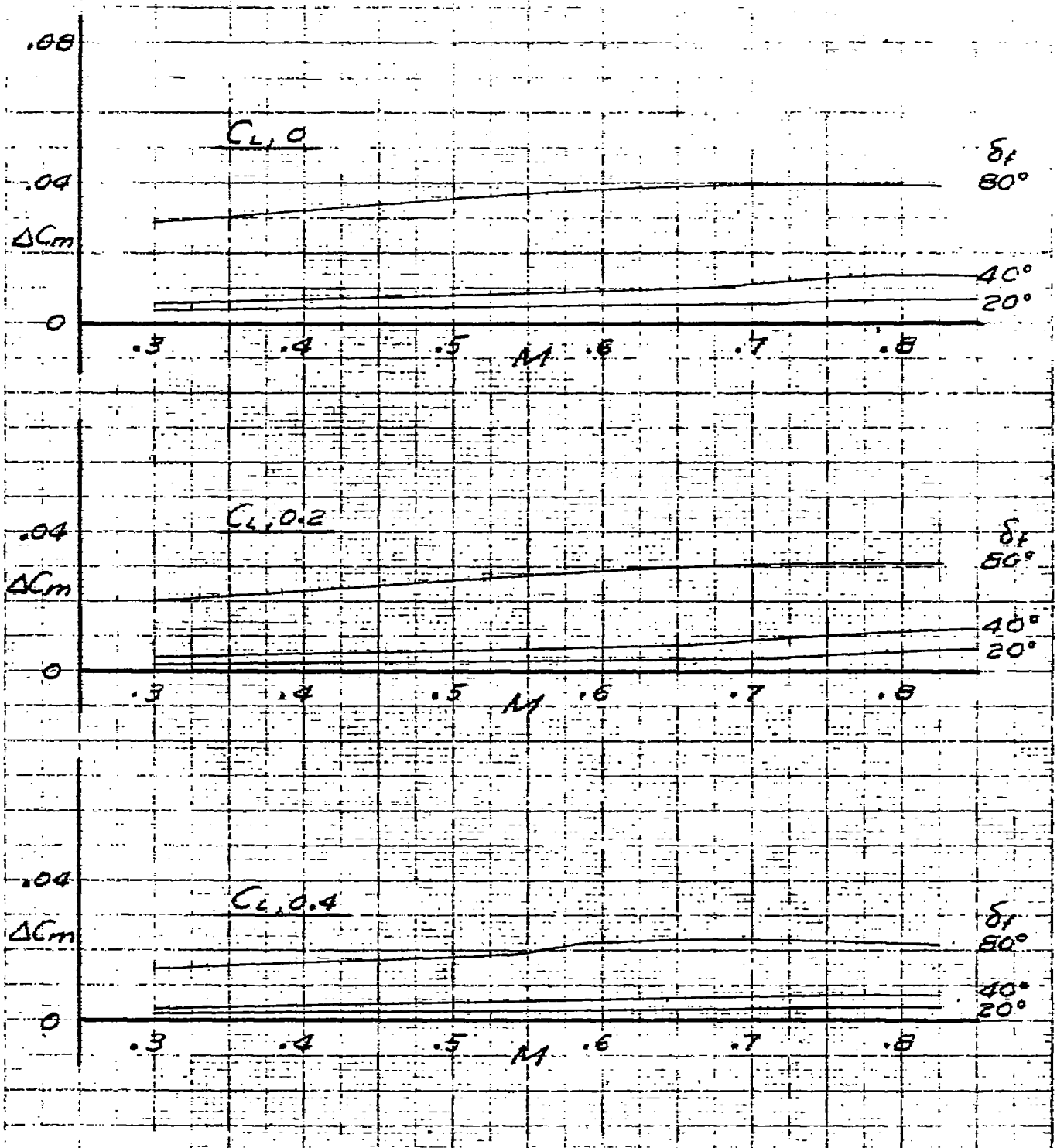

FIGURE 32- THE INCREMENT OF PITCHING-MOMENT COEFFICIENT FROM THE FUSELAGE DIVE-RECOVERY FLAPS FOR THE 1/3-SCALE MODEL OF THE YP-80A AIRPLANE LESS THE TAIL.

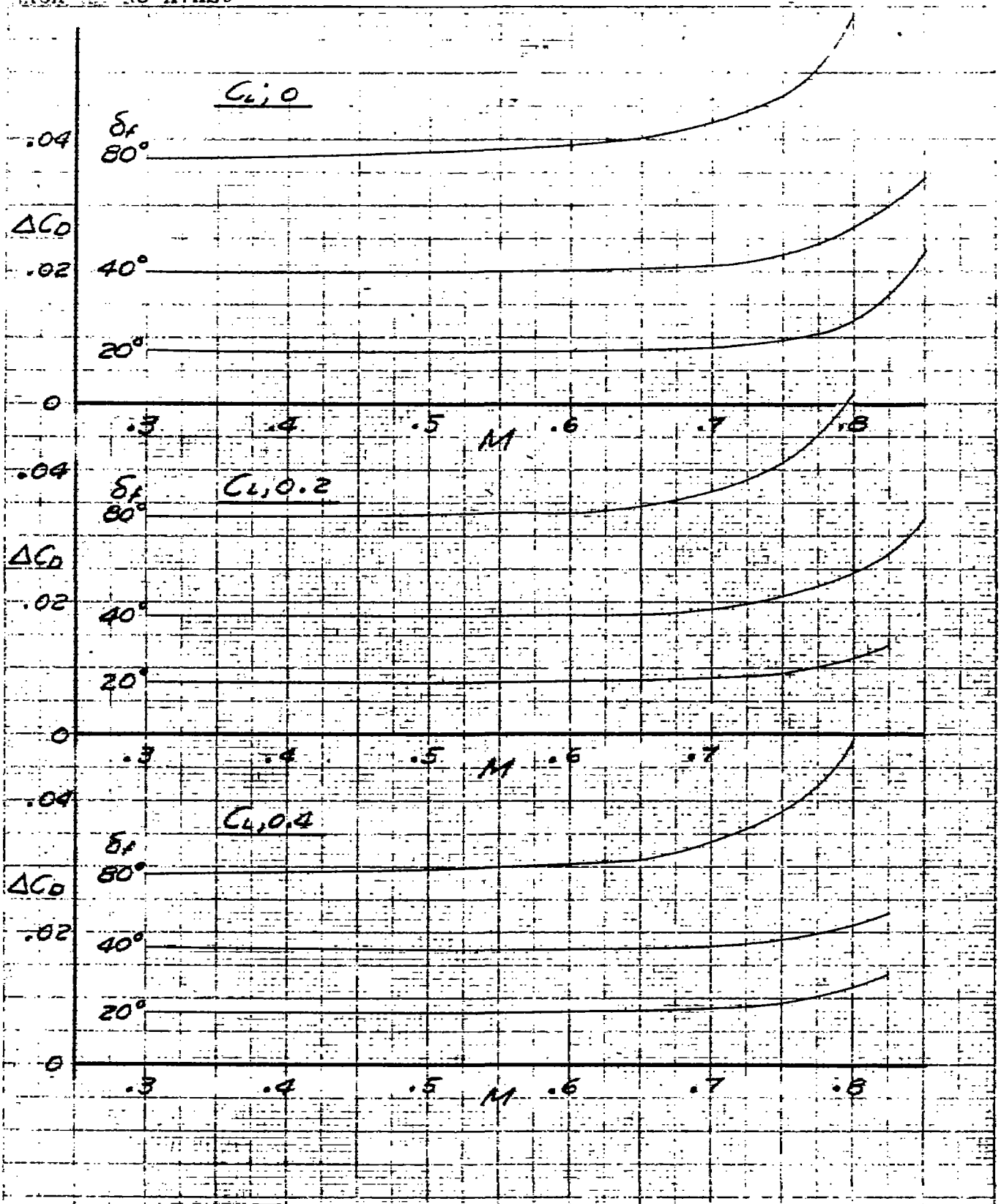

FIGURE 33.—THE INCREMENT OF DRAG COEFFICIENT FROM THE FUSELAGE DIVE-RECOVERY FLAPS FOR THE COMPLETE 1/3-SCALE MODEL OF THE YP-80A AIRPLANE.

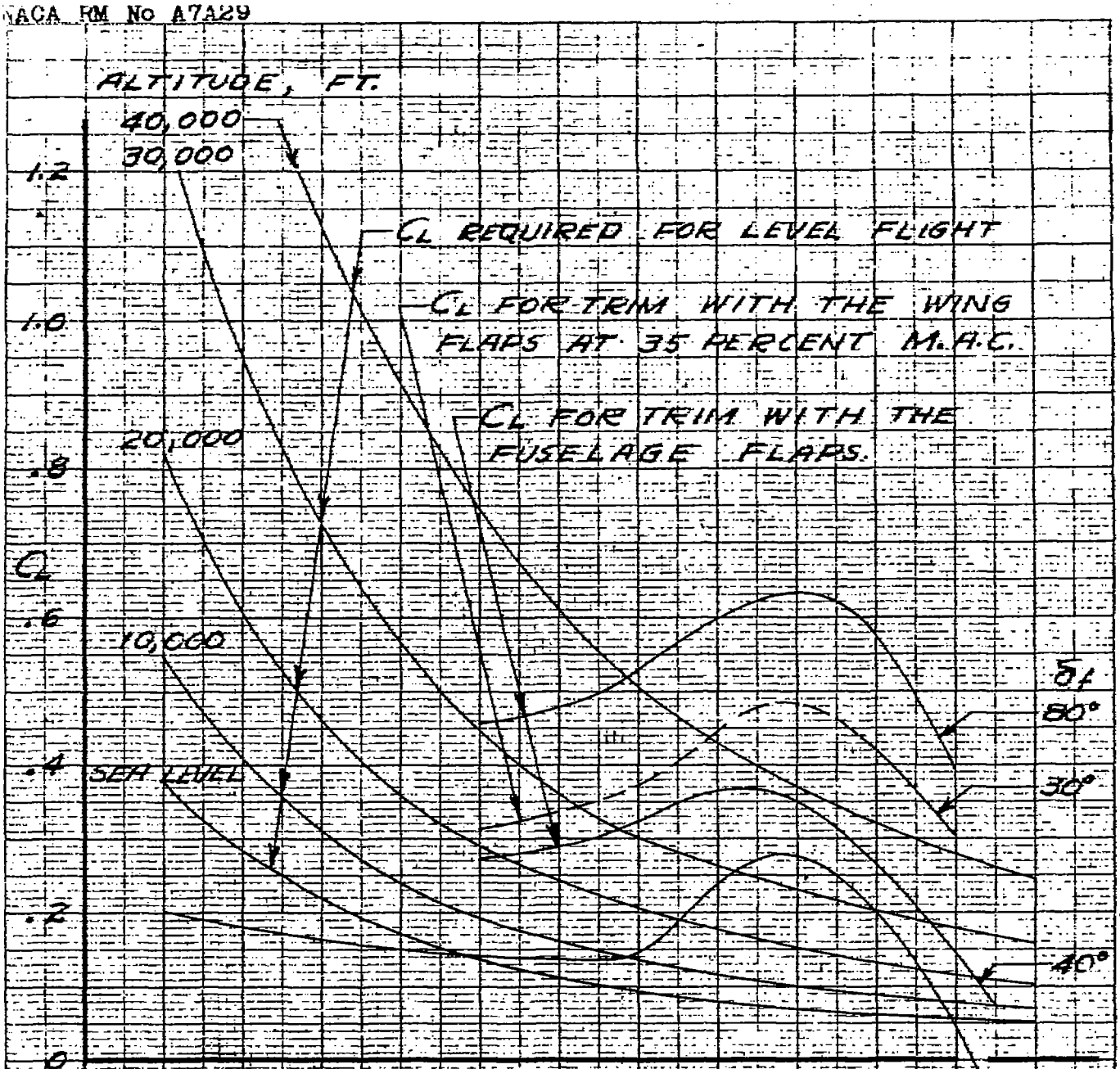

FIGURE 34.- CALCULATED LIFT COEFFICIENT FOR TRIM, STICK FREE, WITH THE DIVE-RECOVERY FLAPS AND THE LIFT COEFFICIENT REQUIRED FOR LEVEL FLIGHT FOR THE YAK 9CH AIRPLANE.